Article

Cell Reports

The Mre11-Nbs1 Interface Is Essential for Viability and Tumor Suppression

Graphical Abstract

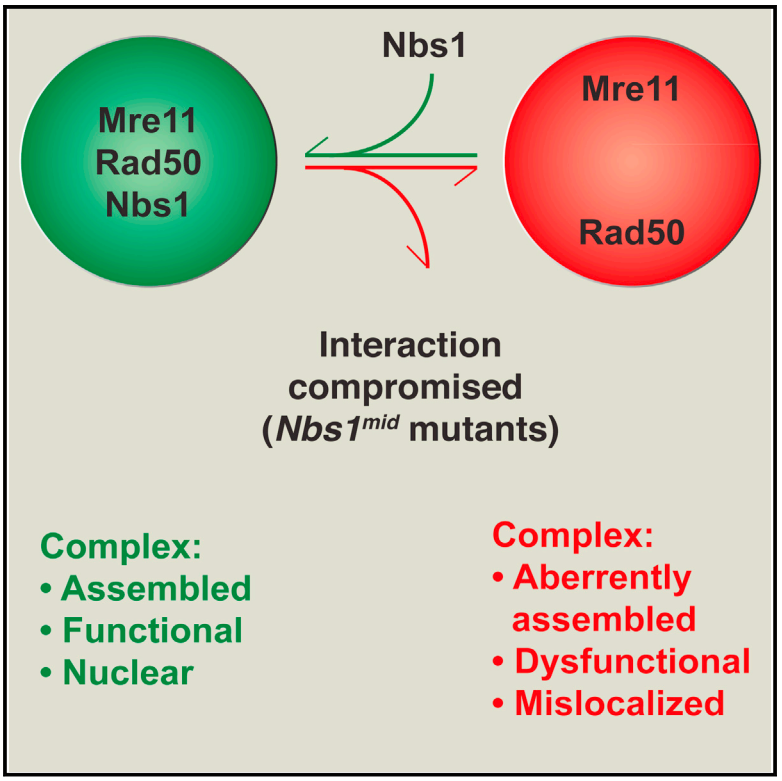

Authors

Jun Hyun Kim, Malgorzata Grosbart, Roopesh Anand, Claire Wyman, Petr Cejka, John H.J. Petrini

Correspondence

petrinij@mskcc.org

In Brief

Kim et al. find that Nbs1 promotes the proper assembly and localization of a complex containing Mre11 and Rad50. Nbs1-mediated assembly is required for the function of the complex, and a 108-amino-acid Nbs1 fragment containing the Mre11 interaction domain is sufficient for this essential role.

Highlights

- TALEN editing used to generate *Nbs1*^{mid} mutant mice altered the Mre11 interaction
- The Mre11-Nbs1 interaction is essential for embryonic viability and DDR
- The Nbs1 minimal fragment (108 amino acid) is sufficient to sustain viability
- Nbs1 is required for proper assembly and localization of Mre11 and Rad50

Kim et al., 2017, Cell Reports *18*, 496–507
January 10, 2017
http://dx.doi.org/10.1016/j.celrep.2016.12.035

OPEN ACCESS
CellPress

Cell Reports
Article

The Mre11-Nbs1 Interface Is Essential for Viability and Tumor Suppression

Jun Hyun Kim,[1] Malgorzata Grosbart,[2,3] Roopesh Anand,[4] Claire Wyman,[2,3] Petr Cejka,[4] and John H.J. Petrini[1,5,*]
[1]Molecular Biology Program, Memorial Sloan Kettering Cancer Center, New York, NY 10021, USA
[2]Department of Molecular Genetics
[3]Department of Radiation Oncology
Erasmus University Medical Center, 3000 Rotterdam, the Netherlands
[4]Institute for Research in Biomedicine, Università della Svizzera Italiana, Via Vincenzo Vela 6, 6500 Bellinzona, Switzerland
[5]Lead Contact
*Correspondence: petrinij@mskcc.org
http://dx.doi.org/10.1016/j.celrep.2016.12.035

SUMMARY

The Mre11 complex (Mre11, Rad50, and Nbs1) is integral to both DNA repair and ataxia telangiectasia mutated (ATM)-dependent DNA damage signaling. All three Mre11 complex components are essential for viability at the cellular and organismal levels. To delineate essential and non-essential Mre11 complex functions that are mediated by Nbs1, we used TALEN-based genome editing to derive *Nbs1* mutant mice (*Nbs1*^{mid} mice), which harbor mutations in the Mre11 interaction domain of Nbs1. *Nbs1*^{mid} alleles that abolished interaction were incompatible with viability. Conversely, a 108-amino-acid Nbs1 fragment comprising the Mre11 interface was sufficient to rescue viability and ATM activation in cultured cells and support differentiation of hematopoietic cells in vivo. These data indicate that the essential role of Nbs1 is via its interaction with Mre11 and that most of the Nbs1 protein is dispensable for Mre11 complex functions and suggest that Mre11 and Rad50 directly activate ATM.

INTRODUCTION

The DNA damage response (DDR) is important for maintaining genomic integrity. It comprises pathways that mediate DNA repair, DNA damage signaling, cell-cycle regulation and apoptosis. Impairment of the DDR is associated with diverse human pathologies such as cancer, neurodegenerative disorders, immune deficiency, and premature aging (Ciccia and Elledge, 2010).

The Mre11 complex—Mre11, Rad50, and Nbs1 (Xrs2 in *S. cerevisiae*)—influences all aspects of the DDR via its role as DNA double-strand break (DSB) sensor as well as its enzymatic and structural roles in DSB repair (Stracker and Petrini, 2011). Each member of the complex has been identified as the underlying basis of chromosome instability syndromes associated with immunodeficiency, radiosensitivity, cell-cycle checkpoint defects, and cancer predisposition (Stracker and Petrini, 2011). These disorders each exhibit decrements in ataxia telangiectasia mutated (ATM) activation or activity, consistent with the idea that the Mre11 complex is required for the activation of ATM. This conclusion is supported by biochemical and genetic analyses in mice, yeast, and human cells (Cerosaletti and Concannon, 2004; Difilippantonio et al., 2005; Schiller et al., 2012; Shull et al., 2009; Stracker et al., 2008; Theunissen et al., 2003; Waltes et al., 2009; Williams et al., 2002).

Whereas Mre11 and Rad50 orthologs are present in Bacteria, Archaea, and Eukaryota, Nbs1 appears to be restricted to Eukaryota. Accordingly, the protein appears to influence functions that are unique to eukaryotic cells. Unlike Mre11 and Rad50, Nbs1 does not appear to bind DNA, nor does it specify enzymatic activities relevant to DNA repair. Nbs1 primarily influences Mre11 complex function by mediating protein interactions via its N- and C-terminal domains that influence DNA repair, subcellular localization, and ATM-dependent checkpoint and apoptotic functions (Cerosaletti and Concannon, 2003; Desai-Mehta et al., 2001; Larsen et al., 2014; Lloyd et al., 2009; Saito and Kobayashi, 2013; Stracker and Petrini, 2011; Williams et al., 2008). The mechanistic basis for Mre11-complex-dependent ATM activation remains unclear. It is notable that the appearance of Nbs1 in eukaryotes coincides with the Mre11 complex's role in promoting DNA damage signaling, as does the Mre11 domain with which Nbs1 interacts. The Mre11 interaction interface of Nbs1 is a bipartite structure comprising Mid1 and Mid2 (Mre11 interaction domain) that is conserved among Nbs1 orthologs (Schiller et al., 2012).

Having previously established that the N and C termini alone and in combination are dispensable for ATM activation (Stracker and Petrini, 2011), we undertook mutagenesis of the Mre11-Nbs1 interface with the goal of impairing the Nbs1-Mre11 interaction while leaving the Nbs1 protein otherwise intact in an effort to define the role of Nbs1 in ATM activation. Using transcription activator-like effector nuclease (TALEN)-based genome editing, we created an allelic series in mice consisting of six mutations (*Nbs1*^{mid}) within Mid2 that impair the interaction between Nbs1 and Mre11 to varying degrees. The most severe mutants abolished the Mre11-Nbs1 interaction, which resulted in the loss of cellular and organismal viability. These data indicate that the Mre11-Nbs1 interaction is essential, and therefore required, for ATM activation.

Complementation of Nbs1-deficient cells with Nbs1 fragments spanning Mid1 and Mid2 rescued the viability of cultured cells

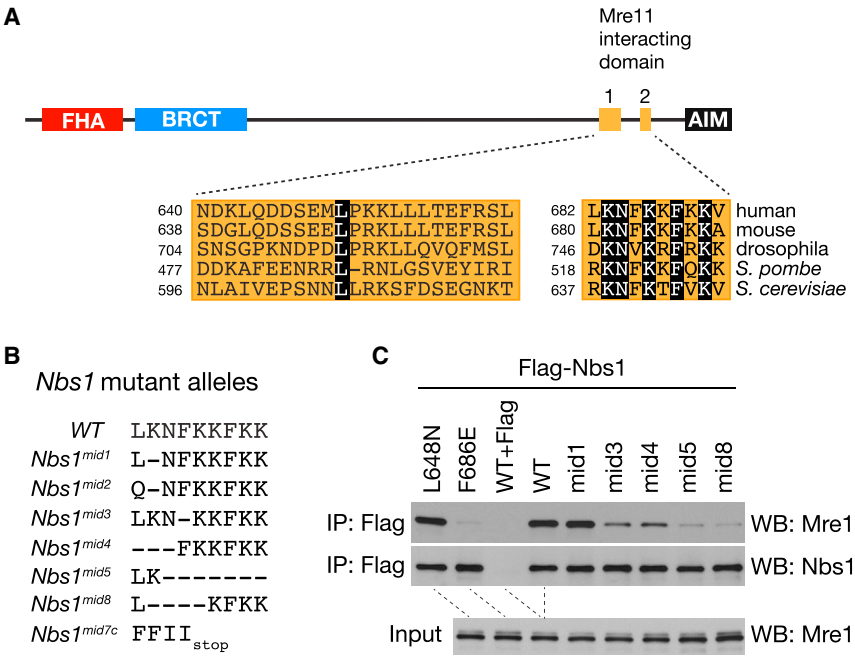

Figure 1. The NFKxFxK Motif in Nbs1 Is Essential for Mouse Embryogenesis

(A) Schematic structure of mammalian Nbs1 protein and sequence alignment of Mre11-interacting domain 1 and 2 among different species. Invariable residues are shown in black boxes. FHA, BRCT, and AIM denote forkhead-associated domain, BRCA1 C-terminal domain, and ATM-interacting motif, respectively.

(B) Sequence of *Nbs1*^{mid} mutant alleles created by TALEN-mediated gene editing. *Nbs1*^{mid7c} is a truncated mutant allele.

(C) Mre11 interaction of different *Nbs1*^{mid} mutants was assessed by immunoprecipitation (IP) by FLAG antibodies followed by western blot for Mre11. FLAG-tagged *WT* or mutant full-length Nbs1 was transiently expressed in MEFs. FLAG peptide (100 μg/mL) was added to the *WT* sample during IP for a FLAG IP control.

(D) Intercrosses of heterozygous *Nbs1*^{mid} mutants. Numbers of pups born are indicated and expected numbers are shown in parenthesis.

D

mutant mice	wildtype	heterozygous	homozygous	total
Nbs1^{mid1}	15 (17.25)	29 (34.5)	25 (17.25)	69
Nbs1^{mid2}	10 (10)	20 (20)	10 (10)	40
Nbs1^{mid3}	24 (23.75)	55 (47.5)	16 (23.75)	95
Nbs1^{mid4}	39 (39.25)	80 (78.5)	38 (39.25)	157
Nbs1^{mid5}	31 (18.75)	44 (37.5)	0 (18.75)	75
Nbs1^{mid8}	28 (18.25)	45 (36.5)	0 (18.25)	73
Nbs1^{mid7c}	6 (4.5)	12 (9)	0 (4.5)	18

Numbers of pups born are indicated and expected numbers are shown in parenthesis.

and hematopoietic cells in vivo. Cells rescued in this manner also exhibited some indices of ATM function. In vitro, the Nbs1 fragments that rescued viability promoted Mre11 dimerization and DNA binding. In addition, they restored the ability of CtIP to activate Mre11 endonuclease activity, a function shown to be dependent on Nbs1. Collectively, these data suggest that the Nbs1-Mre11 interaction is required for proper assembly of the Mre11 complex. Accordingly, that interaction is required for the concerted activities of Mre11 and Rad50 that govern DNA repair and DNA damage signaling and promote viability.

RESULTS

The Evolutionarily Conserved NFKxFxK Motif in Nbs1 Is Essential for Mouse Embryogenesis

The mammalian Nbs1 protein interacts with Mre11 via a bipartite domain near the C terminus, comprising Mid1 and Mid2 (Figure 1A). Mid2 includes a highly conserved NFKxFxK motif, whereas Mid1 is characterized by a single conserved leucine at position 648 of the mouse protein (Figure 1A). We carried out mutagenesis of the *NBS1* cDNA to identify alleles that weakened the Nbs1-Mre11 interaction. Mutation of L648 had a minimal effect on the Mre11-Nbs1 interaction, whereas the interaction was severely impaired by mutation of F686 in Mid2 (Figure 1C). On that basis, we carried out TALEN-based gene editing in mice to induce small deletions within Mid2 and thereby compromise the interaction between Mre11 and Nbs1 (Figure S1A).

We generated seven new *Nbs1*^{mid} mutant mice (*Nbs1*^{mid1}, *Nbs1*^{mid2}, *Nbs1*^{mid3}, *Nbs1*^{mid4}, *Nbs1*^{mid5}, and *Nbs1*^{mid8}) in which the NFKxFxK motif of Mid2 is altered (Figure 1B). The genomic sequences of Nbs1 Exon 13 from founder mutant lines are listed (Figure S1B). These mutations were modeled in cDNA expression constructs. The ability of the corresponding protein products to interact with Mre11 was assessed by co-immunoprecipitation. *Nbs1*^{mid1} was indistinguishable from *WT*, whereas Mre11 interaction was moderately (*Nbs1*^{mid3} and *Nbs1*^{mid4}) to severely impaired (*Nbs1*^{mid5} and *Nbs1*^{mid8}) (Figure 1C). The binding of Nbs1^{mid2} is similar to that of wild-type protein (data not shown). Whereas *Nbs1*$^{mid1/mid1}$, *Nbs1*$^{mid2/mid2}$, *Nbs1*$^{mid3/mid3}$, and *Nbs1*$^{mid4/mid4}$ mice were born at expected Mendelian frequencies, homozygosity for either *Nbs1*^{mid5} or *Nbs1*^{mid8} mutations was lethal, indicating that the Mre11-Nbs1 interaction is essential for embryonic viability (Figure 1D).

Disruption of the Mre11-Nbs1 Interaction Compromises DDR and Promotes Tumorigenesis

The extent to which the Nbs1-Mre11 interaction was impaired scaled with the phenotypic severities observed. We assessed

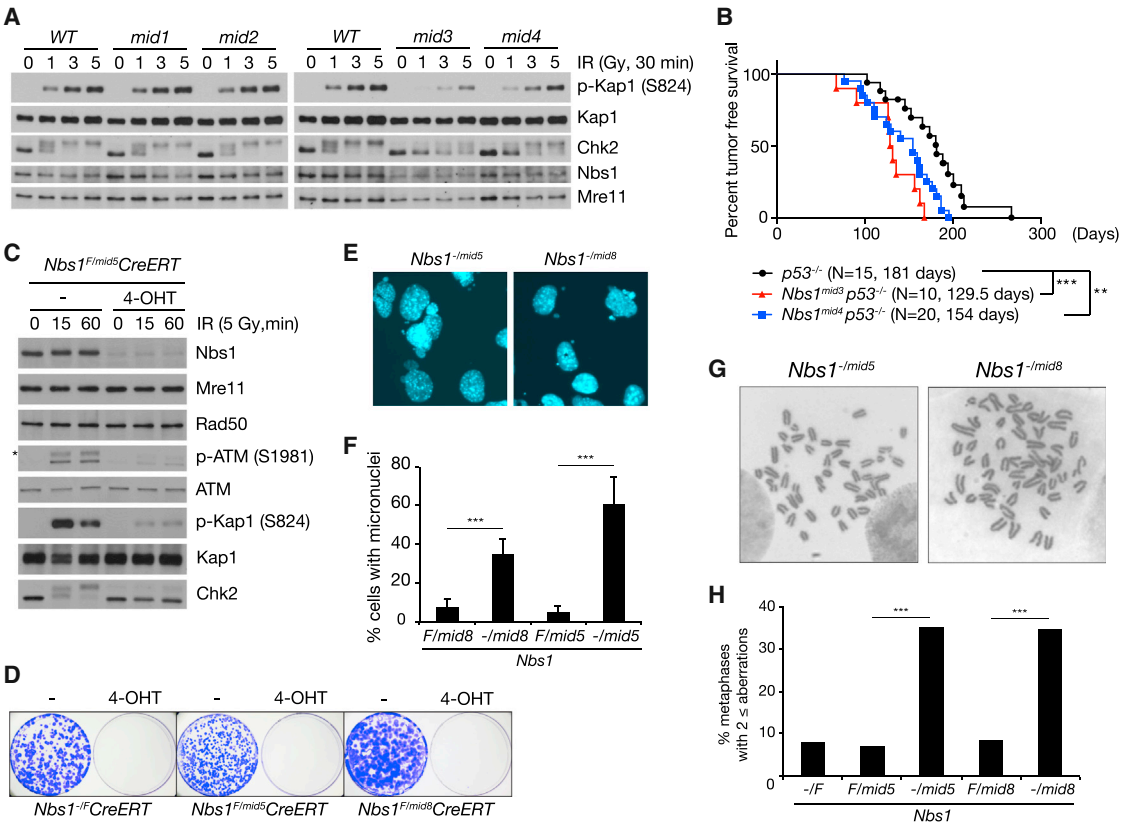

Figure 2. The Mre11-Nbs1 Interaction Is Important for DDR and Tumor Suppression

(A) IR-induced ATM signaling in *WT*, *Nbs1*^{mid1}, *Nbs1*^{mid2}, *Nbs1*^{mid3}, and *Nbs1*^{mid4} thymocytes. ATM signaling was assessed by western blot for the phosphorylation of KAP1 (S824) and hyperphosphorylation of Chk2, which are ATM substrates. Note that Chk2 migrates slowly when hyperphosphorylated.

(B) Mouse tumor free survival. Each data point represents the percent survival of mice with each genotype at a given age. N denotes total number of mice for each genotype and the average age in death in days is shown. p value of double mutants compared to *p53*$^{-/-}$ was determined by Wilcoxon rank sum test (**p < *0.01* and ***p < *0.001*).

(C) ATM signaling in *Nbs1*$^{-/mid5}$ MEFs was assessed by western blot for phospho-ATM (S1981) and the phosphorylation of ATM substrates, KAP1 (S824), and Chk2. The asterisk indicates nonspecific band.

(D) Colony-formation assay to assess cell viability of *Nbs1*$^{-/mid5}$ and *Nbs1*$^{-/mid8}$ alleles in MEFs.

(E) Nuclei were stained with DAPI (4′,6-diamidino-2-phenylindole).

(F) The percentage of nuclei with micronuclei was counted from randomly taken images (mean ± SD, 100 < number [*N*] from seven images). p value was determined by unpaired t test (***p < *0.001*).

(G) Representative chromosome metaphase images of *Nbs1*$^{-/mid5}$ and *Nbs1*$^{-/mid8}$ MEFs.

(H) Percentage of metaphases with aberrations (***p < 0.001, Fisher's exact test, more than 40 metaphases).

the effects of *Nbs1*^{mid} mutations on ATM activation by examining phosphorylation of the ATM substrates Kap1 (S824) and Chk2 following ionizing radiation (IR). In homozygous *Nbs1*^{mid1} and *Nbs1*^{mid2} cells, those endpoints were indistinguishable from *WT*, whereas *Nbs1*^{mid3} and *Nbs1*^{mid4} homozygotes exhibited defects in phosphorylation (Figure 2A). Those mutants also exhibited defects in the G2/M checkpoint, indicative of reduced ATM activation. At 1 hr following treatment with 3 Gy IR, the mitotic index of *WT* cells decreased by 85%–87% (Figure S2A), whereas the decrease was only 64% for *Nbs1*$^{mid3/mid3}$ and 72% for *Nbs1*$^{mid4/mid4}$, consistent with the more severe impairment of Kap1 and Chk2 phosphorylation in *Nbs1*$^{mid3/mid3}$ than *Nbs1*$^{mid4/mid4}$. Similarly, colony-formation assays indicated that IR resistance was reduced in *Nbs1*$^{mid3/mid3}$ and *Nbs1*$^{mid4/mid4}$ cells (Figure S2B).

The defects imparted by *Nbs1*^{mid3} and *Nbs1*^{mid4} increased cancer risk. In our colony, p53-deficient mice present with thymic lymphoma at ~180 days of age. Over a 10-month time course, *Nbs1*$^{mid3/mid3}$ and *Nbs1*$^{mid4/mid4}$ mice did not present with malignancy (data not shown); however, when combined with p53 deficiency, the mean tumor-free survival decreased by 27–50 days relative to *p53*$^{-/-}$ mice (***p < 0.001; *Nbs1*^{mid3} *p53*$^{-/-}$ vs. *p53*$^{-/-}$ and **p < 0.01; *Nbs1*^{mid4} *p53*$^{-/-}$ vs. *p53*$^{-/-}$) (Figure 2B). In addition to reduced latency, the spectrum of tumors arising in double-mutant mice expanded to include leiomyosarcoma, squamous cell carcinoma, hemangiosarcoma, rhabdomyosarcoma, and histiocytic sarcoma (Table S1). We propose that destabilization of the Mre11-Nbs1 interface impairs ATM activation and modifies the *p53*$^{-/-}$ phenotype.

We were unable to establish embryonic fibroblasts homozygous for the *Nbs1*^{mid5} or *Nbs1*^{mid8} alleles. To define the cellular phenotypes of *Nbs1*^{mid5} and *Nbs1*^{mid8}, these mice were crossed with *Nbs1*^{F} mice in which *cre* expression inactivates *NBS1* (Demuth et al., 2004). Following transduction of a tamoxifen (4-OHT)-regulated *cre* recombinase into immortalized mouse embryonic fibroblasts (MEFs) from *Nbs1*$^{F/mid5}$ and *Nbs1*$^{F/mid8}$ mice, 4-OHT was added to the media for 24 hr. *cre*-mediated deletion of *Nbs1*^{F} was evident within 24–48 hr (data not shown), and the remaining Nbs1^{mid5} and Nbs1^{mid8} proteins were present at markedly reduced levels, whereas Mre11 and Rad50 levels were unchanged (Figures 2C and S2C). Colonies of *Nbs1*$^{-/mid5}$ or *Nbs1*$^{-/mid8}$ MEFs were not recovered (Figure 2D), indicating that as in the case of mouse embryos, the Mre11-Nbs1 interaction is essential. 4 days following the induction of *cre* activity (prior to cell death), indices of genome destabilization were evident in both *Nbs1*$^{-/mid5}$ or *Nbs1*$^{-/mid8}$ cells, including micronuclei and chromosome aberrations (Figures 2E–2H). These outcomes resemble those observed upon genetic ablation of *RAD50*, *MRE11*, or *NBS1* (Adelman et al., 2009; Buis et al., 2008; Reina-San-Martin et al., 2005).

ATM activation was assessed in *Nbs1*$^{-/mid5}$ and *Nbs1*$^{-/mid8}$ cells at 4 days following *cre*. IR-induced Kap1 S824 and Chk2 phosphorylation were nearly undetectable in *Nbs1*$^{-/mid5}$ (Figure 2C) and severely attenuated in *Nbs1*$^{-/mid8}$ cells (Figure S2C), suggesting that impairing the Mre11-Nbs1 interaction compromised ATM activation. Accordingly, IR-induced ATM S1987 autophosphorylation, a direct index of ATM activation (Bakkenist and Kastan, 2003; Paull, 2015), was also sharply decreased in *Nbs1*$^{-/mid5}$ cells relative to *Nbs1*$^{F/mid5}$ controls (Figure 2C). As expected, both *Nbs1*^{mid5} and *Nbs1*^{mid8} alleles exhibit defects in the G2/M checkpoint that were considerably more severe than those observed in *Nbs1*$^{mid3/mid3}$ or *Nbs1*$^{mid4/mid4}$ alleles (Figure S2D). These assessments may underestimate the severity of the *Nbs1*$^{-/mid5}$ and *Nbs1*$^{-/mid8}$ phenotypes due to the possible presence of residual Nbs1 protein.

The Nbs1 Minimal Fragment Rescues Nbs1 Deficiency

Previously, a C-terminal truncation of 100 amino acids of human Nbs1 that included Mid1 and Mid2 was unable to rescue viability of Nbs1-deficient mouse cells (Difilippantonio et al., 2005). Data presented here indicate that the presence of an essentially complete Nbs1 protein that is unable to interact with Mre11 was not sufficient for viability or ATM activation. Given that the N and C termini are dispensable, singularly or in combination, for cell viability and ATM activation (Stracker and Petrini, 2011) (data not shown), we used deletional mutagenesis to define the "minimal Nbs1" required to support viability.

Three Nbs1 gene segments encoding N-terminal truncation fragments, all of which also lacked the C-terminal 24 amino acids of Nbs1, were constructed in a retroviral expression vector. The constructs encoded fragments of 388, 188, and 108 amino acids (F2, F3, and F4, respectively) fused to a FLAG epitope and SV40 nuclear localization signal (NLS) at their N termini for nuclear localization (Figure 3A). The Nbs1 gene segments were transduced into *Nbs1*$^{F/F}$ MEFs, and the ability of the encoded fragments to interact with Mre11 was assessed via FLAG immunoprecipitation. All fragments co-immunoprecipitated with Mre11 and Rad50 (Figure 3B). Moreover, F4 which spans just 108 amino acids inclusive of Mid1 and Mid2 displaced full-length Nbs1 from Mre11 and Rad50, arguing that Nbs1 is unlikely to interact with other domains of the Mre11 complex (Figure 3B).

Subsequently, *cre* activity was induced with 4-OHT, and the ability of fragment-containing cells to form colonies was assessed. Whereas no colonies formed from control (vector-transduced) cells, all of the cells expressing F2, F3, and F4 were able to form colonies after 10 days in culture. PCR genotyping and western blot confirmed that the introduced fragments were the sole source of Nbs1 protein remaining in the *Nbs1*$^{-/-}$ cells—the fragments are hereafter designated "rescue fragments" (Figures S3A–S3C). By cloning the cells in this manner and by propagation in culture over the course of several weeks, any contribution from residual Nbs1-proficient (*Nbs1*^{F}) cells to colony formation or subsequent phenotypic assessments was excluded. These data indicated that as few as 108 amino acids of Nbs1 spanning the Mre11-Nbs1 interaction interface are sufficient to sustain the viability of cultured cells.

In addition to sustaining viability, the rescue fragments were able to promote ATM activation in *Nbs1*$^{-/-}$ cells. The phenotypes of Nbs1-fragment-expressing cells were compared to a culture of *Nbs1*$^{F/F}$ cells at 4 days after *cre* induction. Whereas Kap1 S824 phosphorylation was sharply reduced at 0.5 hr after 5 Gy IR in *Nbs1*$^{-/-}$, it was readily evident in F2- and F3-containing cells and, to a lesser extent, in F4 cells (Figure 3C). IR-induced Kap1 S824 phosphorylation of F4 cells was confirmed as ATM-dependent activity by pretreatment with an ATM inhibitor (Figure S3D). Those complemented cells exhibited restoration the G2/M checkpoint. After 1 hr following treatment with 3 Gy IR, the mitotic index of F2-, F3-, and F4-containing *Nbs1*$^{-/-}$ cells decreased by 68%, 66%, and 44%, respectively, while the decrease was only 14% for *ATM*$^{-/-}$ cells (Figure 3D). These data indicate that a substantial degree of ATM-dependent checkpoint function was retained in rescue-fragment-expressing cells. A fragment of human Nbs1 spanning residues 401–754 was previously shown to suppress ATM activation and nuclear localization defects in Nijmegen breakage syndrome (NBS) patient cells (Cerosaletti and Concannon, 2004).

To obtain a quantitative assessment of DDR function in rescue-fragment-containing cells, the frequency of spontaneous chromosome aberrations was assessed. 100% of *Nbs1*$^{-/-}$ cells exhibit widespread chromosome fragility, with more than three aberrations per metaphase spread (Figures 3E and 3F). In contrast, fewer than 21% of F2-, F3-, and F4-containing cells exhibited three or more aberrations (Figure 3F), indicating a substantial degree of residual function.

Nevertheless, rescue-fragment-expressing cells did not phenocopy cells expressing wild-type Nbs1. We observed sharply reduced nuclear localization of Mre11 in F4-containing cells relative to F2 or F3-containing cells (Figure 3G), likely accounting for reduced Kap1 phosphorylation in F4-containing cells. Data from budding yeast and human cells indicate that Xrs2 and Nbs1 are required for nuclear localization of Mre11 and Rad50 (Cerosaletti and Concannon, 2004; Cerosaletti et al., 2006), and enforced nuclear localization of Mre11 in *S. cerevisiae* partially restored function to *xrs2Δ* mutants (Oh et al., 2016; Tsukamoto et al., 2005). F4-containing cells were more sensitive to IR than F2 cells

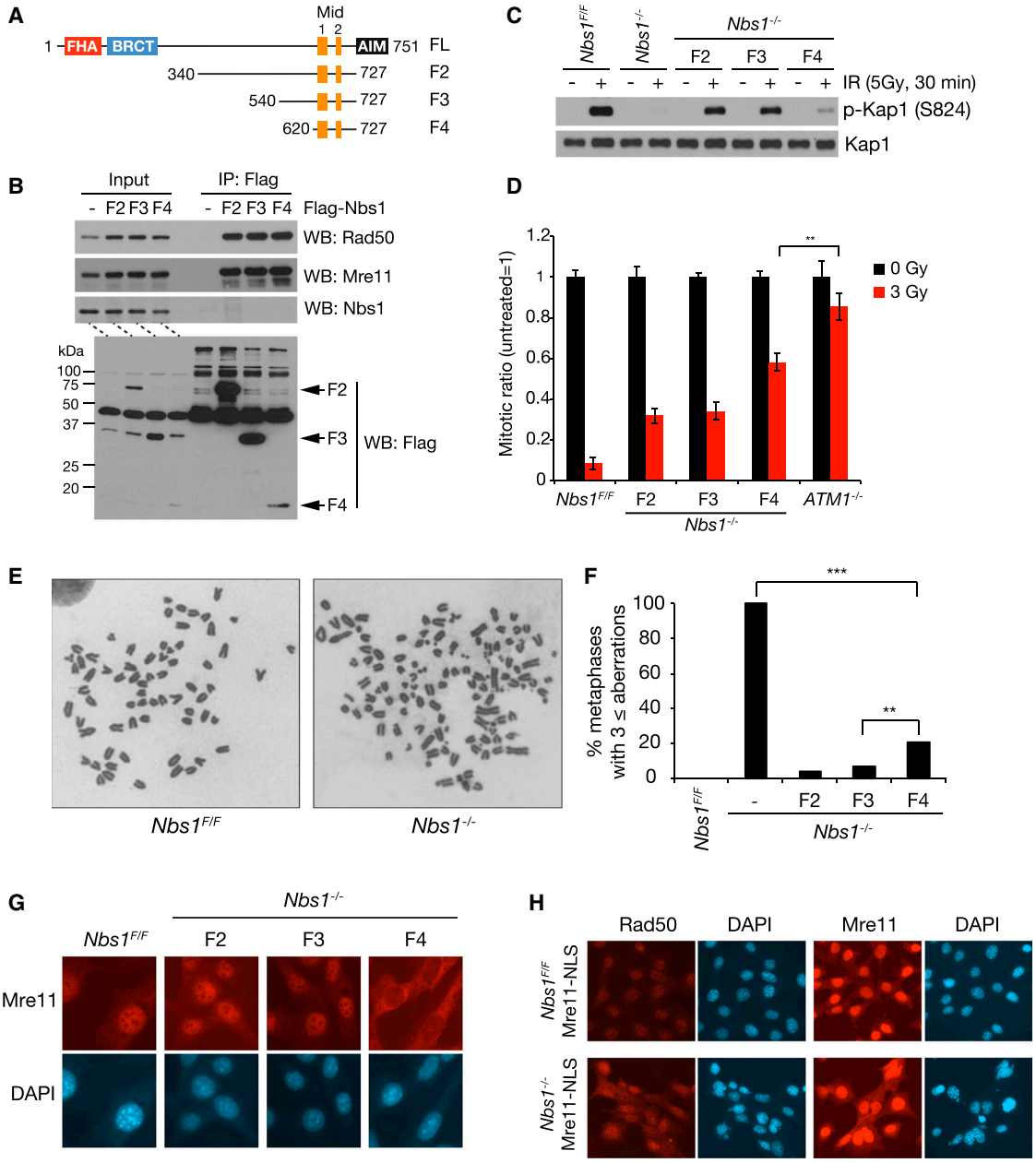

Figure 3. The Nbs1 Minimal Fragment Rescues Nbs1 Deficiency

(A) Structure of Nbs1 fragments used in rescue experiments. Domains are indicated in Figure 1A.

(B) Mre11 interaction of Nbs1 minimal fragments. FLAG-tagged Nbs1 fragments (F2, F3, and F4) were expressed in *Nbs1*$^{F/F}$ MEFs, and immunoprecipitation with FLAG antibodies was performed followed by western blot for Mre11, Rad50, and Nbs1.

(C) IR-induced ATM signaling in *Nbs1*$^{-/-}$ MEFs expressing Nbs1 minimal fragments. As an ATM substrate, phosphorylation of KAP1 (S824) was assessed.

(D) IR-induced G2/M cell-cycle checkpoint of *Nbs1*$^{-/-}$ MEFs expressing Nbs1 minimal fragments. Mitotic cells were detected by measuring mitosis-specific phosphorylation of histone H3 (Ser10). *ATM*$^{-/-}$ MEFs was used for controls. p value was determined by unpaired t test (**$p < 0.01$, mean ± SD, three independent experiments).

(E and F) Metaphase spread of *Nbs1*$^{-/-}$ MEFs expressing Nbs1 minimal fragments. (E) Representative chromosome metaphase images of *Nbs1*$^{F/F}$ and *Nbs1*$^{-/-}$ MEFs. (F) The graph indicates the percent ratio of metaphases with aberrations (**$p < 0.01$ and ***$p < 0.001$, Fisher's exact test, more than 65 metaphases from two independent experiments).

(G) Immunofluorescence cell staining of Mre11 in *Nbs1*$^{-/-}$ MEFs expressing Nbs1 minimal fragments. Nuclei are shown by DAPI (4′,6-diamidino-2-phenylindole) staining.

(H) Immunofluorescence cell staining of Rad50 and Mre11 in *Nbs1*$^{-/-}$ MEFs expressing Mre11-NLS. *Nbs1*$^{-/-}$-Mre11-NLS cells were achieved by treating *Nbs1*$^{F/F}$creERT2-Mre11-NLS cells with 4-OHT treatment. Cells were stained at day 3 after 4-OHT treatment. Nuclei are shown by DAPI (4′,6-diamidino-2-phenylindole) staining.

(Figure S3E), and we reasoned that a contributing factor to the reduced efficiency of F4-dependent restoration of ATM activation might be aberrant localization of Mre11 and Rad50. To determine whether enforced nuclear localization of Mre11 would mitigate the effects of Nbs1 deficiency, we expressed an SV40 NLS-Mre11 cDNA (*Mre11-NLS*) in $Nbs1^{F/F}$ cells. No viable $Nbs1^{-/-}$ *Mre11-NLS*-expressing cells were recovered at 3 weeks, and at 4 days after *cre* induction, Mre11-NLS did not restore IR-induced G2/M checkpoint functions (Figure S4). Consistent with data from human NBS cells (Lakdawala et al., 2008), enforced nuclear localization of Mre11 in $Nbs1^{-/-}$ cells did not restore nuclear localization of Rad50 (Figure 3H).

Biochemical Effects of the Nbs1 Minimal Fragment

These data suggested that Nbs1 influences the stability and assembly of the Mre11 complex in addition to its subcellular localization. To test this interpretation, we examined the effect of human Nbs1 F4 on the biochemical properties of Mre11 in vitro. The human Mre11 core (1–411 amino acids) (Park et al., 2011) was purified and subjected to size exclusion chromatography. Individually, Mre11 and Nbs1 F4 fused to a maltose-binding protein (F4-MBP) primarily appeared as single, monomeric peaks (apparent molecular weight [MW]: 42 kDa for Mre11 and 59 kDa for F4-MBP). When mixed at a 1:1 ratio, we observed a new peak with an apparent molecular weight of 184 kDa, consistent with the co-elution of Mre11 and Nbs1 dimers (i.e., two F4-MBP and two Mre11 cores) (Figures 4A and 4B). The new peak was not observed in F4-*mid5*-MBP in which the NFKKFKK motif is deleted (Figure S5).

F4-MBP also stimulated DNA binding by the Mre11 core. Mre11 binds DNA as a dimer (Williams et al., 2008). We found that the binding of Mre11 to double-stranded DNA (dsDNA) (Figure 4C) or a hairpin (Figure 4D) substrate was stimulated by Nbs1 F4 in electrophoretic mobility shift assays (EMSAs). Supershifting induced by MBP antisera confirmed that the Mre11-DNA complex contains Nbs1 (Figure 4D).

We next examined the effect of F4-MBP on Mre11 nuclease activity. Phosphorylated CtIP has recently been shown to promote Mre11 endonuclease in a manner that depends on Nbs1 (Anand et al., 2016). The Mre11-Rad50 complex was incubated with a 70-bp radiolabeled dsDNA substrate, the ends of which were blocked by streptavidin to prevent exonucleolytic degradation (Figure 4E). In the absence of F4-MBP, or in the presence of the non-interacting F4-*mid5*-MBP fragment (Figure 4F), CtIP did not promote endonucleolytic cleavage by Mre11 (Figures 4G and 4H). In contrast, wild-type F4-MBP with phosphorylated CtIP promoted the endonuclease of Mre11-Rad50 (Figure 4H).

To further examine the hypothesis that Nbs1 mediates proper assembly of Mre11 and Rad50, we carried out scanning force microscopy (SFM). Previous SFM analysis revealed a stoichiometry of two or four Nbs1 proteins per M_2R_2 complex (van der Linden et al., 2009). However, the addition of two or four Nbs1 proteins to the globular domain of M_2R_2 obscured possible structural rearrangement. The minimal Nbs1 fragment identified here allowed analysis of Mre11 changes in complex architecture by SFM imaging. The M_2R_2 complex is characterized by a single globular domain (Mre11 + Rad50 ATPase domains) with two protruding coiled coils (Figure 5A). The coiled coils are usually apart but 32% of the time appear to be linked by the zinc-hook domains at their apexes (de Jager et al., 2004; Moreno-Herrero et al., 2005).

To assess the effect of F4 on Mre11 complex assembly, the full-length human M_2R_2 complex was incubated at a 1:1 molar ratio with F4-MBP or F4-*mid5*-MBP (non-binding mutant) before imaging. A striking rearrangement of the Mre11 globular domain was induced in the presence of the F4 peptide, with the globular domain appearing as two distinct but linked globular objects (Figure 5B). The proportion of Mre11 complexes with this conformation increases from 12% to 58% in the presence of the F4 peptide but does not significantly change in the presence of the control F4-*mid5* peptide (Figure 5C). This separation into two distinct globular objects is accompanied by an increase in width of the globular domain (Figure 5D), consistent different conformations of related Mre11 complexes captured in X-ray crystallography studies (Wyman et al., 2011). Incubation with the F4 peptide also notably changed the conformation of the coiled coils. In the presence of the F4 peptide, Mre11 complexes exhibited a notable increase in complexes with coiled coils linked via the zinc-hook apexes (Figures 5E and 5F). These data suggest that that Nbs1 influences nanoscale arrangement of Rad50 and Mre11 globular domains with consequent influence on conformational flexibility of the Rad50 coiled coils favoring dimerization of the zinc hooks. Collectively, these data strongly support the view that Nbs1's influence on the physical disposition of the Mre11 complex constitutes its essential function and that this influence underlies its requirement for nuclear localization, cell viability, and ATM activation.

$Nbs1^{-/-}$ Fetal Liver Cells Reconstitute the Hematopoietic System upon Nbs1 Minimal Fragment Expression

Immortalized cells are likely more tolerant of genotoxic stress than constituents of tissues in vivo. To determine whether the rescue fragments would sustain viability in vivo, we assessed their ability to support the differentiation of lymphocytes. Previous analyses indicated that the Mre11 complex is required for lymphocyte development (Balestrini et al., 2016; Callén et al., 2007; Deriano et al., 2009; Reina-San-Martin et al., 2004). $Nbs1^{F/F}$ mice were crossed to *vavCre* mice, which express *cre* recombinase in hematopoietic stem cells (HSCs) (Stadtfeld and Graf, 2005). Hematopoietic Nbs1 deficiency resulted in perinatal lethality due to lack of bone marrow development (Figure S6).

Fetal liver cells (FLCs) from embryonic day 13.5 (E13.5) embryos were isolated and transduced with *Nbs1* rescue fragment encoding in an IRES-GFP murine stem cell virus (MSCV) retrovirus prior to transplantation into lethally irradiated mice as depicted (Figure 6A). At 10 weeks after transplantation, spleen was isolated and assessed for GFP-positive cells. Although we did not observe complete reconstitution, GFP-positive, B220-positive cells comprised 6% of splenocytes (Figure 6B). The percentages of GFP-positive, B220-positive cells may underestimate the degree of reconstitution by rescue-fragment-containing HSCs due to silencing of the MSCV retrovirus during hematopoietic differentiation as observed previously (Cherry et al., 2000). The Mre11 complex is dispensable for viability of quiescent cells

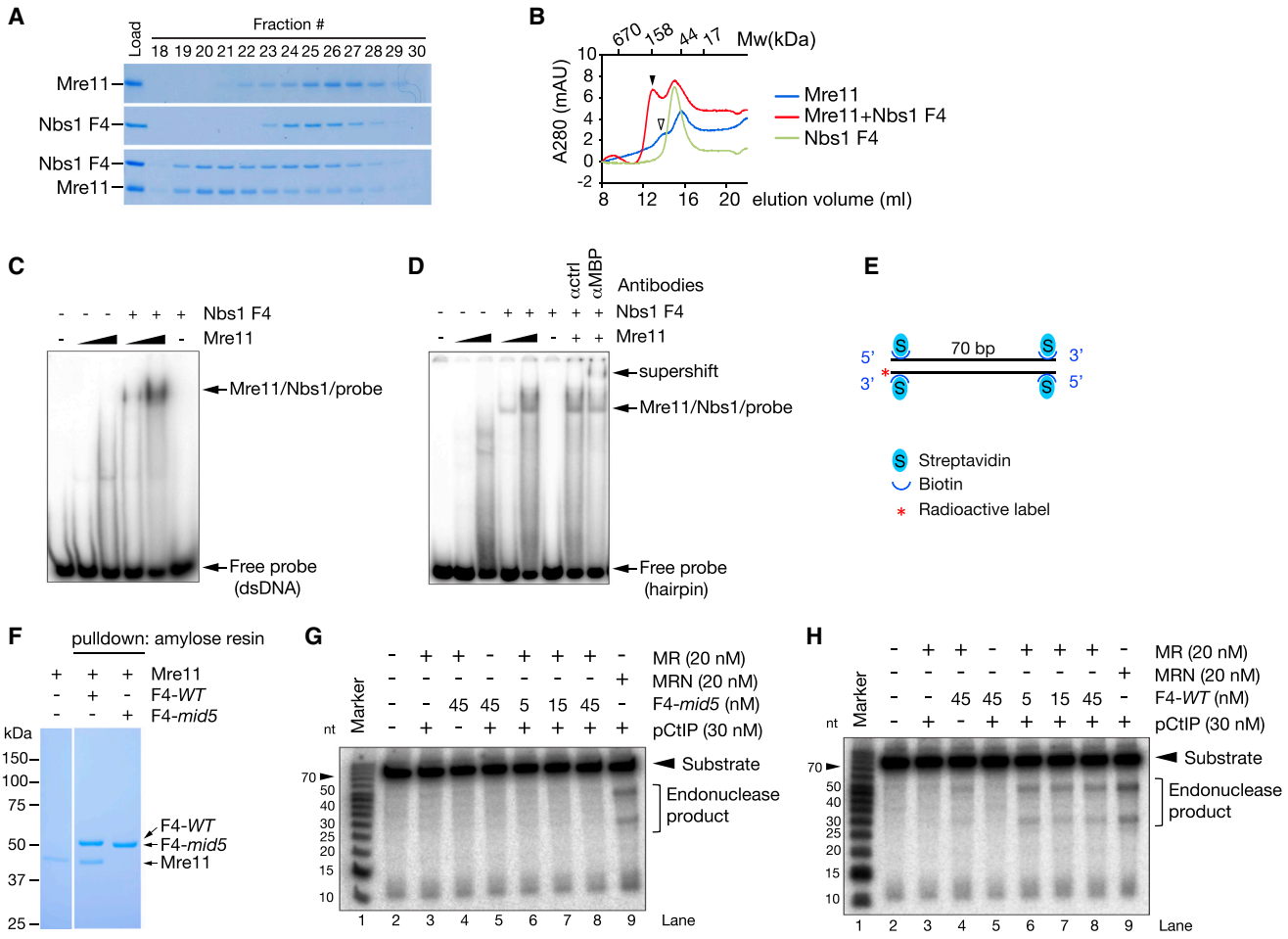

Figure 4. The Nbs1 Minimal Fragment Promotes Mre11 Dimer Formation, Mre11 DNA Binding, and Nuclease Activity

(A) Gel filtration of the Mre11 and Nbs1 complex by Superdex 200 in the presence of 1 mM $MnCl_2$. An equimolar mixture of human Mre11 (1–411 amino acids) and Nbs1 (F4) protein was used at 0.5 μM.

(B) Elution traced of a gel filtration experiment. Molecular weight was estimated by a gel filtration standard. Arrowheads indicate higher molecular weight complex; Mre11/Nbs1 dimers (closed) and Mre11 dimer (open).

(C and D) DNA binding of Mre11. Electrophoretic mobility shift assay (EMSA) was performed using purified human Mre11 (1–411 amino acids, 1 μM and 5 μM) and Nbs1 (F4, 5 μM) proteins with 10 nM of end-labeled double-stranded (C) or hairpin (D) DNA probe. Supershift was performed using 1 μg MBP antibody. All EMSA reactions were performed in the absence of Mn^{2+}.

(E) Mre11 endonuclease assay probe. The 3′ end-labeled 70-bp dsDNA is blocked at both ends with streptavidin.

(F) Amylose pull-down assay for Mre11 binding of F4 and F4-*mid5* protein. An equimolar mixture of human Mre11 (1–411 amino acids) and Nbs1 (MBP-F4-*WT* or MBP-F4-*mid5*) protein was incubated with amylose resin at 1 μM in the presence of 1 mM $MnCl_2$, and the interaction was visualized by Coomassie-blue-stained SDS-PAGE.

(G and H) Endonuclease assay with Mre11/Rad50/phosphorylated CtIP with F4-*mid5* (G) or F4-*WT* (H). M, R, and pCtIP denote Mre11, Rad50, and phosphorylated CtIP, respectively.

(Adelman et al., 2009); hence, silencing of F4 expression may be tolerated because splenocytes are largely quiescent.

PCR genotyping confirmed that recipient mice contain differentiated cells derived from Nbs1 fragment containing $Nbs1^{-/-}$ FLCs and that the fragment-encoding construct is present; the $Nbs1^{F}$ allele was not detected (Figure 6C). This confirms that this rescue is not by remaining undeleted $Nbs1^{F}$ allele in donor FLCs. No reconstitution was observed in control mice transduced with FLCs lacking the rescue fragments (data not shown). These data indicate that as with transformed cells, the 108 amino acids spanning the Mre11 interaction interface of Nbs1 (F4; Figure 3A) are sufficient to promote viability in vivo and, moreover, that minimal Nbs1 fragment was sufficiently functional to support differentiation of HSCs into splenic B cells.

DISCUSSION

To examine the role of Nbs1 in Mre11 complex functions, we undertook mutagenesis of Nbs1 in an attempt to weaken the interaction with Mre11 and thereby examine the functionality of the

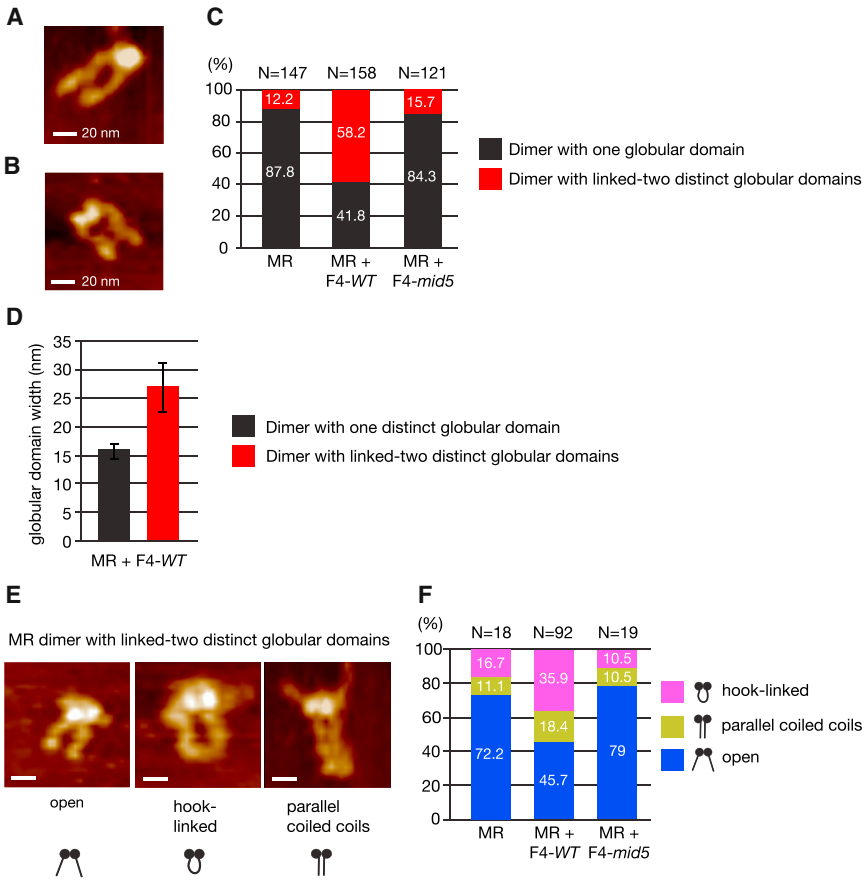

Figure 5. The Nbs1 Minimal Fragment Causes Rearrangement of MR Architecture

(A and B) SFM image examples of MR complexes appearing with one globular domain (A) or appearing with globular domain with two distinguishable parts (B).

(C) Distribution of MR molecules based on globular domain arrangement, alone and in the presence of Nbs1 F4-*WT* or -*mid5*.

(D) The two forms of MR illustrated in (A) and (B) can be distinguished based on the width of their globular domain. The width for molecules with one globular domain and two distinct linked globular domains is plotted (average of n = 66 and n = 92, respectively, ± SD).

(E) SFM image examples of coiled-coil arrangements classified for complexes with two distinct linked globular domains (scale bar, 20 nM).

(F) Distribution of the coiled-coil arrangement among MR complexes with two distinct linked globular domains, alone and in the presence of Nbs1 F4-*WT* or -*mid5*.

M and R denote Mre11 and Rad50, respectively.

core Mre11-Rad50 complex disassociated from Nbs1. Mutations that disrupted Mre11 interaction caused inviability. Hence, the presence of a non-interacting but otherwise intact Nbs1 protomer was not sufficient for viability, establishing that Nbs1 interaction per se is essential. Conversely, we found that 108 amino acids of Nbs1 spanning the Mre11 interaction domain were sufficient to promote cell viability. Although ATM activation was reduced in that setting, it was not abolished. Collectively, the data strongly argue that ATM activation is not directly dependent on Nbs1. Instead, we propose that essential functions of Nbs1 are to ensure proper assembly and subcellular localization of the Mre11 complex, which in turn promotes viability and influences ATM activation by Mre11 and Rad50.

The Role of Nbs1 in the Mre11 Complex: Essential Functions

Nbs1 clearly mediates essential as well as non-essential functions. With respect to the former, the data presented here indicate that the Mre11-Nbs1 interaction is specifically required for cellular and organismal viability. The levels of Mre11 and Rad50 protein were not changed in *Nbs1*^{mid} mutant cells. Hence, it is the loss of interaction, rather than global destabilization of Mre11 complex components that accounts for the loss of viability in non-interacting *Nbs1*^{mid} mutants. Further, this emphasizes the fact that Mid2 (the conserved NFKxFxK motif, which was the target of the TALEN-based mutagenesis) is the major determinant of Nbs1's association with the Mre11 complex. These data are consistent with the finding that the *human Nbs1*^{tr645} allele in which the C-terminal 100 amino acids of Nbs1 were deleted was unable to support viability of mouse embryos (Difilippantonio et al., 2005).

What are the essential functions of Nbs1 in the Mre11 complex? First, it is clear that the nuclear localization of Mre11 is influenced by Nbs1, but this does not solely depend on the Mre11 interaction domain. Mre11 complex mislocalization is observed in human NBS and A-TLD cells, as well as in *Nbs1*$^{\Delta B/\Delta B}$ and *Mre11*$^{ATLD1/ATLD1}$ mouse models of those human mutations, neither of which harbor alterations in their respective interaction domains (Carney et al., 1998; Difilippantonio et al., 2005; Reina-San-Martin et al., 2005; Stewart et al., 1999; Williams et al., 2002). Nbs1 and Mre11 levels are reduced in those settings, raising the possibility that the stoichiometry of complex components may also influence nuclear localization. Alternatively, those mutations may disrupt as-yet-undescribed interactions required for nuclear localization.

Nevertheless, promoting nuclear localization of Mre11 and Rad50 is likely not the only function of Nbs1 required for viability. Enforced nuclear localization by Mre11-NLS could not restore nuclear localization of Rad50 in human NBS cells (Lakdawala et al., 2008), nor did it compensate for Nbs1 deficiency in MEFs (Figure 3H). The data presented here are most consistent with the interpretation that Nbs1 influences the assembly and disposition of the complex. Supporting that view, we showed that dimerization and DNA binding by the N-terminal 411-amino-acid core of Mre11 was enhanced by the F4 fragment (Figures 4A–4D), although it is likely that dimeric assemblies of full-length Mre11 may exhibit greater stability. Further support comes from the fact that only in the presence of Nbs1 or the minimal fragment is

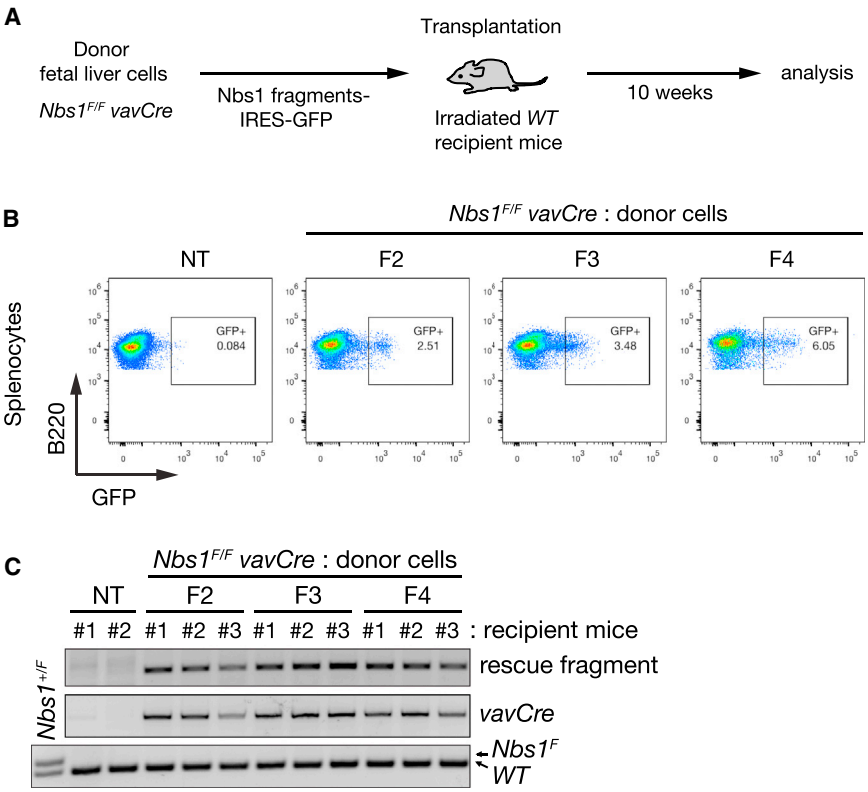

Figure 6. Hematopoietic Reconstitution by the Nbs1 Minimal Fragment

(A) Experimental scheme of fetal liver cell transplantation.

(B) Flow cytometry analysis of splenocytes from recipient mice 10 weeks post-transplantation. For B cells, B220^{+} cells were gated from total splenocytes and plotted by GFP signal. Plots shown here are representative of recipient mice from each group of Nbs1 fragments.

(C) PCR genotyping of splenocytes for an exogenous Nbs1 fragment, *vavCre* and *Nbs1*^{F} allele, which is donor-FLC specific. *Nbs1*$^{+/F}$ MEFs were used for PCR control for the *Nbs1*^{F} allele. NT denotes control mouse.

CtIP able to stimulate Mre11 endonucleolytic cleavage (Figure 4H). Finally, scanning force microscopy analysis reveals that in the presence of Nbs1 (whether minimal fragment F4 or the full-length Nbs1 protein), the Mre11-Rad50 complex exhibits substantial structural differences in the disposition of Mre11 and Rad50 in the globular domain, the path of the coiled coils, and the association of the apical (presumably hook) domains of Rad50. These physical data resonate with genetic data indicating that mutations in Rad50 exert effects on regions distal to the altered residues (Al-Ahmadie et al., 2014; Hohl et al., 2011, 2015; Hopfner et al., 2002). On the basis of these findings, we favor the view that Nbs1 functions as a chaperone to promote proper assembly of the complex, which is a prerequisite for its enzymatic and DNA-binding functions as well as for determining its subcellular localization.

The Role of Nbs1 in the Mre11 Complex: Non-essential Functions

The non-essential functions of Nbs1 have been illuminated by genetic analyses in human cells and mice. Nbs1 contains N-terminal forkhead-associated (FHA) and BRCA1 C-terminal (BRCT) domains, which are disrupted in the canonical *Nbs1*$^{657\Delta5}$ allele inherited by NBS patients and the corresponding *Nbs1*$^{\Delta B}$ allele in mice. Those mutants exhibit defects in DSB end resection, DNA repair, and cell-cycle checkpoint activation, presumably due to the loss of protein interactions mediated by those domains (Alt et al., 2005; Chapman and Jackson, 2008; Kobayashi et al., 2002; Larsen et al., 2014; Lloyd et al., 2009; Maser et al., 2001; Melander et al., 2008; Morishima et al., 2007; Spycher et al., 2008; Williams et al., 2009; Wu et al., 2008, 2012). However, human and mouse cells lacking those domains are viable and retain the ability to activate ATM (Difilippantonio et al., 2005; Williams et al., 2002). Deletion of the Nbs1 C terminus (the *Nbs1*$^{\Delta C}$ allele), which has been reported to bind ATM (Falck et al., 2005; You et al., 2005), had no effect on ATM activation or cell viability but is required for ATM-dependent apoptosis (Stracker et al., 2007).

The *Nbs1*$^{\Delta BC}$ allele is a composite of the *Nbs1*$^{\Delta B}$ and *Nbs1*$^{\Delta C}$. The outcomes of *Nbs1*$^{\Delta B}$ and *Nbs1*$^{\Delta C}$ are simply additive in *Nbs1*$^{\Delta BC/\Delta BC}$ mice rather than synergistic; the phenotypic outcomes attributable to *Nbs1*$^{\Delta B}$ and *Nbs1*$^{\Delta C}$ are unchanged in the composite *Nbs1*$^{\Delta BC}$ (Shull et al., 2009; Stracker et al., 2007). Therefore, we propose that Nbs1 serves as a platform for Mre11 complex assembly and the recruitment of ATM substrates to enhance access of the activated kinase to substrates that govern ATM- and Nbs1-dependent functions. In this context, we draw a distinction between ATM activation and ATM activities: in the former circumstance, a properly assembled and localized complex is required for ATM activation, whereas in the latter, Nbs1 potentiates ATM activity by promoting access of the active kinase to its downstream effectors.

Although viability and ATM activation are lost upon genetic ablation of Nbs1, the protein does not appear to influence those outcomes directly. Rather, its association with Mre11 (and so Rad50) via its conserved interaction interface appears to influence both the subcellular localization and the proper assembly of the Mre11 complex, which in turn accounts for its influence on viability as well as ATM activation (Figure 7). Indeed, most of the Nbs1 protein, save for the Mre11 interaction interface, is dispensable for viability as well as ATM activation. Therefore, the mechanism(s) underlying ATM activation would appear to be mediated by Mre11 and Rad50. Notably, ATM appears to interact with Rad50 in vitro (Lee and Paull, 2005), and recent genetic and biochemical analyses have shown that Rad50 influences the activation of ATM or its budding yeast ortholog, Tel1 (Al-Ahmadie et al., 2014; Deshpande et al., 2014; Hohl et al., 2015). These data underlie the speculation that Rad50 is likely to be the proximal effector of ATM activation.

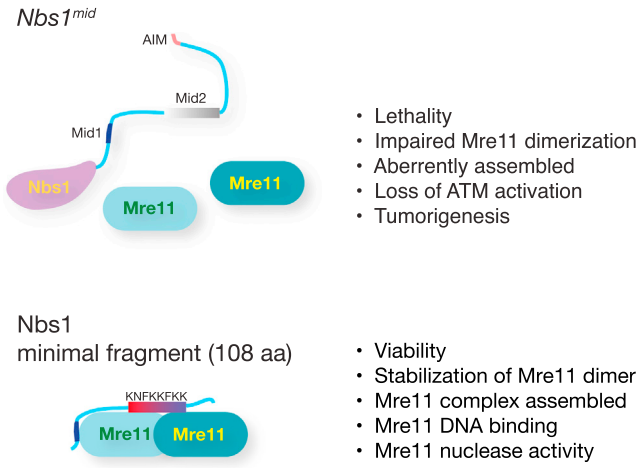

Figure 7. The Mre11 Interaction Domain of Nbs1 Is Necessary and Sufficient for Mre11 Complex Functions

Disruption of the Mre11-Nbs1 interaction results in cellular and organismal lethality and increased tumorigenesis due to a defect in Mre11 complex function. An Nbs1 minimal fragment spanning just the Mre11-Nbs1 interaction interface is sufficient to sustain the viability of cells and stabilize Mre11 dimer and Mre11 DNA binding and nuclease activity. These data indicate an essential role for Nbs1 is via its interaction with Mre11 and that most of the Nbs1 protein is dispensable for Mre11 complex functions. Mid1, Mid2, and AIM denote Mre11-interacting domain 1, Mre11-interacting domain 2, and ATM interacting motif, respectively.

Manipulation of the DDR for therapeutic benefit offers significant potential (O'Connor, 2015). Accordingly, understanding of ATM activation is an important issue. This study thus provides important mechanistic insight toward that goal by defining the role of Nbs1 in promoting Mre11 complex functions in the DDR.

EXPERIMENTAL PROCEDURES

For detailed protocols of cell lines, cellular assay, fetal liver cell transplantation, immunofluorescence staining, and histopathology, see Supplemental Experimental Procedures.

Mice

Nbs1^{mid} mice were generated by help of the Memorial Sloan Kettering Mouse Genetics core. Detailed protocol will be provided upon request. *Nbs1$^{\Delta B}$* mice were previously described (Williams et al., 2002), and *Nbs1^{F}* and *vavCre* mice were kindly provided by Zhao-Qi Wang (Fritz Lipmann Institute, Germany) and Hans-Guido Wendel (Memorial Sloan Kettering Cancer Center, USA), respectively. The Institutional Animal Care and Use Committee of Memorial Sloan Kettering Cancer Center approved all protocols for animal use.

Protein Purification and Analysis

Bacterial expression vector for N-terminal his-tagged human Mre11 (2–411 amino acids) was gifted from Dr. John Tainer (Lawrence Berkeley National Laboratory, USA). With C-terminal his tag, human Nbs1 (F4; 622–729 amino acids) was constructed in pMAL vector (New England Biolabs) for N-terminal MBP tag for its solubility. See Supplemental Experimental Procedures for the purification, EMSA, and nuclease assay.

SFM Analysis

For SFM analysis of MR/NBS1 F4-*WT* or -*mid5* complexes, Mre11-Rad50 (MR) protein and Nbs1 F4 fragment were mixed in reaction buffer (20 mM Tris-HCl [pH 8], 0.1 M EDTA, 0.2 M NaCl, and 2 mM DTT) at a molar ratio 1:1 (8 nM of MR to 8 nM F4-*WT* or -*mid5*) in total volume of 20 μL and incubated for 5 min on ice. The samples were then diluted five times in final volume of 20 μL in reaction buffer and deposited on freshly cleaved mica. After a 1-min incubation at room temperature, the mica was washed with milliQ water and dried with filtered air. Samples were imaged at room temperature and humidity with a Nanoscope VIII (Digital Instruments) operating in tapping mode. Type NHC-W silicon tips with resonance frequency 310–372 kHz were obtained from Nanosensors (Veeco Instruments). Images were collected at 2.5 × 2.5 μm, standard resolution 512 lines × 512 rows, and processed only by flattening to remove background slope. Images were quantified first by identifying MR complexes by visual inspection where molecules consisting a large globular domain with two protruding coiled coils were identified as M_2R_2. These were further classified based on the arrangement of globular domains as dimers with one globular domain or dimers with two distinct linked globular domains. The latter were further categorized according to the arrangement of coiled coils as open, parallel, or hook-linked. The frequency of the different forms was expressed as percentage of total molecules counted. The width of individual globular domains was determined using SFMetrics V4e software (Sánchez and Wyman, 2015) by manually measuring the longest axis across the globular domain.

Statistical Analysis

Statistical significance was analyzed by unpaired t test, Fisher's exact test, or Wilcoxon rank sum test and expressed as a p value as indicated in the figure legends.

SUPPLEMENTAL INFORMATION

Supplemental Information includes Supplemental Experimental Procedures, six figures, and one table and can be found with this article online at http://dx.doi.org/10.1016/j.celrep.2016.12.035.

AUTHOR CONTRIBUTIONS

J.H.K., M.G., and R.A. performed the experiments and analyzed the data. J.H.K., C.W., P.C., and J.H.J.P. designed the experiments. J.H.K. and J.H.J.P. wrote the paper.

ACKNOWLEDGMENTS

We thank John Tainer, Julien Lafrance-Vanasse, Titia de Lange, Hans-Guido Wendel, and Zhao-Qi Wang for reagents, cells, and mice. Members of the J.H.J.P. laboratory, including Thomas J. Kelly, provided helpful comments and suggestions throughout the course of this study. We are very grateful to Willie Mark and Peter Romanienko for designing and carrying out TALEN-based mutagenesis. This work was supported by the Geoffrey Beene Center at MSK Cancer Center, NIH grants GM59413 (to J.H.J.P.) and 1F32 GM105296 (to J.H.K.), and MSK Cancer Center core grant P30 CA008748.

Received: May 14, 2016
Revised: November 4, 2016
Accepted: December 12, 2016
Published: January 3, 2017

REFERENCES

Adelman, C.A., De, S., and Petrini, J.H. (2009). Rad50 is dispensable for the maintenance and viability of postmitotic tissues. Mol. Cell. Biol. *29*, 483–492.

Al-Ahmadie, H., Iyer, G., Hohl, M., Asthana, S., Inagaki, A., Schultz, N., Hanrahan, A.J., Scott, S.N., Brannon, A.R., McDermott, G.C., et al. (2014). Synthetic lethality in ATM-deficient RAD50-mutant tumors underlies outlier response to cancer therapy. Cancer Discov. *4*, 1014–1021.

Alt, J.R., Bouska, A., Fernandez, M.R., Cerny, R.L., Xiao, H., and Eischen, C.M. (2005). Mdm2 binds to Nbs1 at sites of DNA damage and regulates double strand break repair. J. Biol. Chem. *280*, 18771–18781.

Anand, R., Ranjha, L., Cannavo, E., and Cejka, P. (2016). Phosphorylated CtIP functions as a co-factor of the MRE11-RAD50-NBS1 endonuclease in DNA end resection. Mol. Cell *64*, 940–950.

Bakkenist, C.J., and Kastan, M.B. (2003). DNA damage activates ATM through intermolecular autophosphorylation and dimer dissociation. Nature *421*, 499–506.

Balestrini, A., Nicolas, L., Yang-Lott, K., Guryanova, O.A., Levine, R.L., Bassing, C.H., Chaudhuri, J., and Petrini, J.H. (2016). Defining ATM-independent functions of the Mre11 complex with a novel mouse model. Mol. Cancer Res. *4*, 185–195.

Buis, J., Wu, Y., Deng, Y., Leddon, J., Westfield, G., Eckersdorff, M., Sekiguchi, J.M., Chang, S., and Ferguson, D.O. (2008). Mre11 nuclease activity has essential roles in DNA repair and genomic stability distinct from ATM activation. Cell *135*, 85–96.

Callén, E., Jankovic, M., Difilippantonio, S., Daniel, J.A., Chen, H.T., Celeste, A., Pellegrini, M., McBride, K., Wangsa, D., Bredemeyer, A.L., et al. (2007). ATM prevents the persistence and propagation of chromosome breaks in lymphocytes. Cell *130*, 63–75.

Carney, J.P., Maser, R.S., Olivares, H., Davis, E.M., Le Beau, M., Yates, J.R., 3rd, Hays, L., Morgan, W.F., and Petrini, J.H. (1998). The hMre11/hRad50 protein complex and Nijmegen breakage syndrome: linkage of double-strand break repair to the cellular DNA damage response. Cell *93*, 477–486.

Cerosaletti, K.M., and Concannon, P. (2003). Nibrin forkhead-associated domain and breast cancer C-terminal domain are both required for nuclear focus formation and phosphorylation. J. Biol. Chem. *278*, 21944–21951.

Cerosaletti, K., and Concannon, P. (2004). Independent roles for nibrin and Mre11-Rad50 in the activation and function of Atm. J. Biol. Chem. *279*, 38813–38819.

Cerosaletti, K., Wright, J., and Concannon, P. (2006). Active role for nibrin in the kinetics of atm activation. Mol. Cell. Biol. *26*, 1691–1699.

Chapman, J.R., and Jackson, S.P. (2008). Phospho-dependent interactions between NBS1 and MDC1 mediate chromatin retention of the MRN complex at sites of DNA damage. EMBO Rep. *9*, 795–801.

Cherry, S.R., Biniszkiewicz, D., van Parijs, L., Baltimore, D., and Jaenisch, R. (2000). Retroviral expression in embryonic stem cells and hematopoietic stem cells. Mol. Cell. Biol. *20*, 7419–7426.

Ciccia, A., and Elledge, S.J. (2010). The DNA damage response: making it safe to play with knives. Mol. Cell *40*, 179–204.

de Jager, M., Trujillo, K.M., Sung, P., Hopfner, K.P., Carney, J.P., Tainer, J.A., Connelly, J.C., Leach, D.R., Kanaar, R., and Wyman, C. (2004). Differential arrangements of conserved building blocks among homologs of the Rad50/Mre11 DNA repair protein complex. J. Mol. Biol. *339*, 937–949.

Demuth, I., Frappart, P.O., Hildebrand, G., Melchers, A., Lobitz, S., Stöckl, L., Varon, R., Herceg, Z., Sperling, K., Wang, Z.Q., and Digweed, M. (2004). An inducible null mutant murine model of Nijmegen breakage syndrome proves the essential function of NBS1 in chromosomal stability and cell viability. Hum. Mol. Genet. *13*, 2385–2397.

Deriano, L., Stracker, T.H., Baker, A., Petrini, J.H., and Roth, D.B. (2009). Roles for NBS1 in alternative nonhomologous end-joining of V(D)J recombination intermediates. Mol. Cell *34*, 13–25.

Desai-Mehta, A., Cerosaletti, K.M., and Concannon, P. (2001). Distinct functional domains of nibrin mediate Mre11 binding, focus formation, and nuclear localization. Mol. Cell. Biol. *21*, 2184–2191.

Deshpande, R.A., Williams, G.J., Limbo, O., Williams, R.S., Kuhnlein, J., Lee, J.H., Classen, S., Guenther, G., Russell, P., Tainer, J.A., and Paull, T.T. (2014). ATP-driven Rad50 conformations regulate DNA tethering, end resection, and ATM checkpoint signaling. EMBO J. *33*, 482–500.

Difilippantonio, S., Celeste, A., Fernandez-Capetillo, O., Chen, H.T., Reina San Martin, B., Van Laethem, F., Yang, Y.P., Petukhova, G.V., Eckhaus, M., Feigenbaum, L., et al. (2005). Role of Nbs1 in the activation of the Atm kinase revealed in humanized mouse models. Nat. Cell Biol. *7*, 675–685.

Falck, J., Coates, J., and Jackson, S.P. (2005). Conserved modes of recruitment of ATM, ATR and DNA-PKcs to sites of DNA damage. Nature *434*, 605–611.

Hohl, M., Kwon, Y., Galván, S.M., Xue, X., Tous, C., Aguilera, A., Sung, P., and Petrini, J.H. (2011). The Rad50 coiled-coil domain is indispensable for Mre11 complex functions. Nat. Struct. Mol. Biol. *18*, 1124–1131.

Hohl, M., Kochańczyk, T., Tous, C., Aguilera, A., Krężel, A., and Petrini, J.H. (2015). Interdependence of the rad50 hook and globular domain functions. Mol. Cell *57*, 479–491.

Hopfner, K.P., Craig, L., Moncalian, G., Zinkel, R.A., Usui, T., Owen, B.A., Karcher, A., Henderson, B., Bodmer, J.L., McMurray, C.T., et al. (2002). The Rad50 zinc-hook is a structure joining Mre11 complexes in DNA recombination and repair. Nature *418*, 562–566.

Kobayashi, J., Tauchi, H., Sakamoto, S., Nakamura, A., Morishima, K., Matsuura, S., Kobayashi, T., Tamai, K., Tanimoto, K., and Komatsu, K. (2002). NBS1 localizes to gamma-H2AX foci through interaction with the FHA/BRCT domain. Curr. Biol. *12*, 1846–1851.

Lakdawala, S.S., Schwartz, R.A., Ferenchak, K., Carson, C.T., McSharry, B.P., Wilkinson, G.W., and Weitzman, M.D. (2008). Differential requirements of the C terminus of Nbs1 in suppressing adenovirus DNA replication and promoting concatemer formation. J. Virol. *82*, 8362–8372.

Larsen, D.H., Hari, F., Clapperton, J.A., Gwerder, M., Gutsche, K., Altmeyer, M., Jungmichel, S., Toledo, L.I., Fink, D., Rask, M.B., et al. (2014). The NBS1-Treacle complex controls ribosomal RNA transcription in response to DNA damage. Nat. Cell Biol. *16*, 792–803.

Lee, J.H., and Paull, T.T. (2005). ATM activation by DNA double-strand breaks through the Mre11-Rad50-Nbs1 complex. Science *308*, 551–554.

Lloyd, J., Chapman, J.R., Clapperton, J.A., Haire, L.F., Hartsuiker, E., Li, J., Carr, A.M., Jackson, S.P., and Smerdon, S.J. (2009). A supramodular FHA/BRCT-repeat architecture mediates Nbs1 adaptor function in response to DNA damage. Cell *139*, 100–111.

Maser, R.S., Mirzoeva, O.K., Wells, J., Olivares, H., Williams, B.R., Zinkel, R.A., Farnham, P.J., and Petrini, J.H. (2001). Mre11 complex and DNA replication: linkage to E2F and sites of DNA synthesis. Mol. Cell. Biol. *21*, 6006–6016.

Melander, F., Bekker-Jensen, S., Falck, J., Bartek, J., Mailand, N., and Lukas, J. (2008). Phosphorylation of SDT repeats in the MDC1 N terminus triggers retention of NBS1 at the DNA damage-modified chromatin. J. Cell Biol. *181*, 213–226.

Moreno-Herrero, F., de Jager, M., Dekker, N.H., Kanaar, R., Wyman, C., and Dekker, C. (2005). Mesoscale conformational changes in the DNA-repair complex Rad50/Mre11/Nbs1 upon binding DNA. Nature *437*, 440–443.

Morishima, K., Sakamoto, S., Kobayashi, J., Izumi, H., Suda, T., Matsumoto, Y., Tauchi, H., Ide, H., Komatsu, K., and Matsuura, S. (2007). TopBP1 associates with NBS1 and is involved in homologous recombination repair. Biochem. Biophys. Res. Commun. *362*, 872–879.

O'Connor, M.J. (2015). Targeting the DNA Damage Response in Cancer. Mol. Cell *60*, 547–560.

Oh, J., Al-Zain, A., Cannavo, E., Cejka, P., and Symington, L.S. (2016). Xrs2 dependent and independent functions of the Mre11-Rad50 complex. Mol. Cell *64*, 405–415.

Park, Y.B., Chae, J., Kim, Y.C., and Cho, Y. (2011). Crystal structure of human Mre11: understanding tumorigenic mutations. Structure *19*, 1591–1602.

Paull, T.T. (2015). Mechanisms of ATM activation. Annu. Rev. Biochem. *84*, 711–738.

Reina-San-Martin, B., Chen, H.T., Nussenzweig, A., and Nussenzweig, M.C. (2004). ATM is required for efficient recombination between immunoglobulin switch regions. J. Exp. Med. *200*, 1103–1110.

Reina-San-Martin, B., Nussenzweig, M.C., Nussenzweig, A., and Difilippantonio, S. (2005). Genomic instability, endoreduplication, and diminished Ig class-switch recombination in B cells lacking Nbs1. Proc. Natl. Acad. Sci. USA *102*, 1590–1595.

Saito, Y.F.H., and Kobayashi, J. (2013). Role of NBS1 in DNA damage response and its relationship with cancer development. Transl. Cancer Res. *2*, 178–189.

Sánchez, H., and Wyman, C. (2015). SFMetrics: an analysis tool for scanning force microscopy images of biomolecules. BMC Bioinformatics *16*, 27.

Schiller, C.B., Lammens, K., Guerini, I., Coordes, B., Feldmann, H., Schlauderer, F., Möckel, C., Schele, A., Strässer, K., Jackson, S.P., and Hopfner, K.P. (2012). Structure of Mre11-Nbs1 complex yields insights into ataxia-telangiectasia-like disease mutations and DNA damage signaling. Nat. Struct. Mol. Biol. *19*, 693–700.

Shull, E.R., Lee, Y., Nakane, H., Stracker, T.H., Zhao, J., Russell, H.R., Petrini, J.H., and McKinnon, P.J. (2009). Differential DNA damage signaling accounts for distinct neural apoptotic responses in ATLD and NBS. Genes Dev. *23*, 171–180.

Spycher, C., Miller, E.S., Townsend, K., Pavic, L., Morrice, N.A., Janscak, P., Stewart, G.S., and Stucki, M. (2008). Constitutive phosphorylation of MDC1 physically links the MRE11-RAD50-NBS1 complex to damaged chromatin. J. Cell Biol. *181*, 227–240.

Stadtfeld, M., and Graf, T. (2005). Assessing the role of hematopoietic plasticity for endothelial and hepatocyte development by non-invasive lineage tracing. Development *132*, 203–213.

Stewart, G.S., Maser, R.S., Stankovic, T., Bressan, D.A., Kaplan, M.I., Jaspers, N.G., Raams, A., Byrd, P.J., Petrini, J.H., and Taylor, A.M. (1999). The DNA double-strand break repair gene hMRE11 is mutated in individuals with an ataxia-telangiectasia-like disorder. Cell *99*, 577–587.

Stracker, T.H., and Petrini, J.H. (2011). The MRE11 complex: starting from the ends. Nat. Rev. Mol. Cell Biol. *12*, 90–103.

Stracker, T.H., Morales, M., Couto, S.S., Hussein, H., and Petrini, J.H. (2007). The carboxy terminus of NBS1 is required for induction of apoptosis by the MRE11 complex. Nature *447*, 218–221.

Stracker, T.H., Couto, S.S., Cordon-Cardo, C., Matos, T., and Petrini, J.H. (2008). Chk2 suppresses the oncogenic potential of DNA replication-associated DNA damage. Mol. Cell *31*, 21–32.

Theunissen, J.W., Kaplan, M.I., Hunt, P.A., Williams, B.R., Ferguson, D.O., Alt, F.W., and Petrini, J.H. (2003). Checkpoint failure and chromosomal instability without lymphomagenesis in Mre11(ATLD1/ATLD1) mice. Mol. Cell *12*, 1511–1523.

Tsukamoto, Y., Mitsuoka, C., Terasawa, M., Ogawa, H., and Ogawa, T. (2005). Xrs2p regulates Mre11p translocation to the nucleus and plays a role in telomere elongation and meiotic recombination. Mol. Biol. Cell *16*, 597–608.

van der Linden, E., Sanchez, H., Kinoshita, E., Kanaar, R., and Wyman, C. (2009). RAD50 and NBS1 form a stable complex functional in DNA binding and tethering. Nucleic Acids Res. *37*, 1580–1588.

Waltes, R., Kalb, R., Gatei, M., Kijas, A.W., Stumm, M., Sobeck, A., Wieland, B., Varon, R., Lerenthal, Y., Lavin, M.F., et al. (2009). Human RAD50 deficiency in a Nijmegen breakage syndrome-like disorder. Am. J. Hum. Genet. *84*, 605–616.

Williams, B.R., Mirzoeva, O.K., Morgan, W.F., Lin, J., Dunnick, W., and Petrini, J.H. (2002). A murine model of Nijmegen breakage syndrome. Curr. Biol. *12*, 648–653.

Williams, R.S., Moncalian, G., Williams, J.S., Yamada, Y., Limbo, O., Shin, D.S., Groocock, L.M., Cahill, D., Hitomi, C., Guenther, G., et al. (2008). Mre11 dimers coordinate DNA end bridging and nuclease processing in double-strand-break repair. Cell *135*, 97–109.

Williams, R.S., Dodson, G.E., Limbo, O., Yamada, Y., Williams, J.S., Guenther, G., Classen, S., Glover, J.N., Iwasaki, H., Russell, P., and Tainer, J.A. (2009). Nbs1 flexibly tethers Ctp1 and Mre11-Rad50 to coordinate DNA double-strand break processing and repair. Cell *139*, 87–99.

Wu, L., Luo, K., Lou, Z., and Chen, J. (2008). MDC1 regulates intra-S-phase checkpoint by targeting NBS1 to DNA double-strand breaks. Proc. Natl. Acad. Sci. USA *105*, 11200–11205.

Wu, J., Zhang, X., Zhang, L., Wu, C.Y., Rezaeian, A.H., Chan, C.H., Li, J.M., Wang, J., Gao, Y., Han, F., et al. (2012). Skp2 E3 ligase integrates ATM activation and homologous recombination repair by ubiquitinating NBS1. Mol. Cell *46*, 351–361.

Wyman, C., Lebbink, J., and Kanaar, R. (2011). Mre11-Rad50 complex crystals suggest molecular calisthenics. DNA Repair (Amst.) *10*, 1066–1070.

You, Z., Chahwan, C., Bailis, J., Hunter, T., and Russell, P. (2005). ATM activation and its recruitment to damaged DNA require binding to the C terminus of Nbs1. Mol. Cell. Biol. *25*, 5363–5379.

Cell Reports, Volume *18*

Supplemental Information

The Mre11-Nbs1 Interface Is Essential for Viability and Tumor Suppression

Jun Hyun Kim, Malgorzata Grosbart, Roopesh Anand, Claire Wyman, Petr Cejka, and John H.J. Petrini

Supplemental Information

The Mre11-Nbs1 interface is essential for viability and tumor suppression

Jun Hyun Kim[1], Malgorzata Grosbart[2,3], Roopesh Anand[4] Claire Wyman[2,3], Petr Cejka[4], and John H.J. Petrini[1]*

[1]Molecular Biology Program,

Memorial Sloan-Kettering Cancer Center, New York, NY10021, USA

Department of [2]Molecular Genetics and [3]Radiation Oncology,

Erasmus University Medical Center, 3000 CA Rotterdam, The Netherlands

[4]Institute for Research in Biomedicine, Università della Svizzera Italiana, Via Vincenzo Vela 6, 6500 Bellinzona, Switzerland

*Correspondence: petrinij@mskcc.org

A

B

```
amino acid    T  S  R  N  L  C  V  N  E  C  G  P  L  K  N  F  K  K  F  K  K
Nbs1 WT       ACCTCCAGAAATCTATGTGTAAATGAATGTGGTCCACTGAAGAATTTCAAGAAATTCAAGAAGGTAGGTGT
mid1 (Δ3)     ACCTCCAGAAATCTATGTGTAAATGAATGTGGTCCACTGAA---TTTCAAGAAATTCAAGAAGGTAGGTGT
mid2 (Δ3)     ACCTCCAGAAATCTATGTGTAAATGAATGTGGTCCAC---AGAATTTCAAGAAATTCAAGAAGGTAGGTGT
mid3 (Δ3)     ACCTCCAGAAATCTATGTGTAAATGAATGTGGTCCACTGAAGAA---CAAGAAATTCAAGAAGGTAGGTGT
mid4 (Δ9)     ACCTCCAGAAATCTATGTGTAAATGAATGTGGTCCA---------TTCAAGAAATTCAAGAAGGTAGGTGT
mid5 (Δ21)    ACCTCCAGAAATCTATGTGTAAATGAATGTGGTCCACTGAA--------------------GGTAGGTGT
mid6 (Ins1)   ACCTCCAGAAATCTATGTGTAAATGAATGTGGTCCACTGAAGAATTTTCAAGAAATTCAAGAAGGTAGGTGT
mid7c(Ins10)  ACCTCCAGAAATCTATGTGTAAATGAATGTGGTCCATTTTTTATAATATAAAATAAGCAAGAAATTCAAGAAGGTAGGTGT
mid8 (Δ12)    ACCTCCAGAAATCTATGTGTAAATGAATGTGGTCCACTGAA------------ATTCAAGAAGGTAGGTGT
```

XmnI : GAANN|NNTTC
TALEN binding sequences
Mre11 interacting domain 2 sequences : KNFKKFKK

Figure S1. TALEN targeting for *Nbs1*^{mid} mutant mouse lines, Related to Figure1.
(A) Binding sites of two recombinant TALE nucleases (TALEN) targeting Mre11-interacting domain 2 of mouse Nbs1 gene. (B) Examples of genomic sequences of *Nbs1*^{mid} mutant mouse lines. Binding sites of two recombinant TALEN are indicated in blue color. XmnI restriction enzyme site that was used for initial diagnosis of gene editing by TALEN is indicated in red color. The sequence of Mre11 interacting domain 2 is indicated in green color.

Figure S2

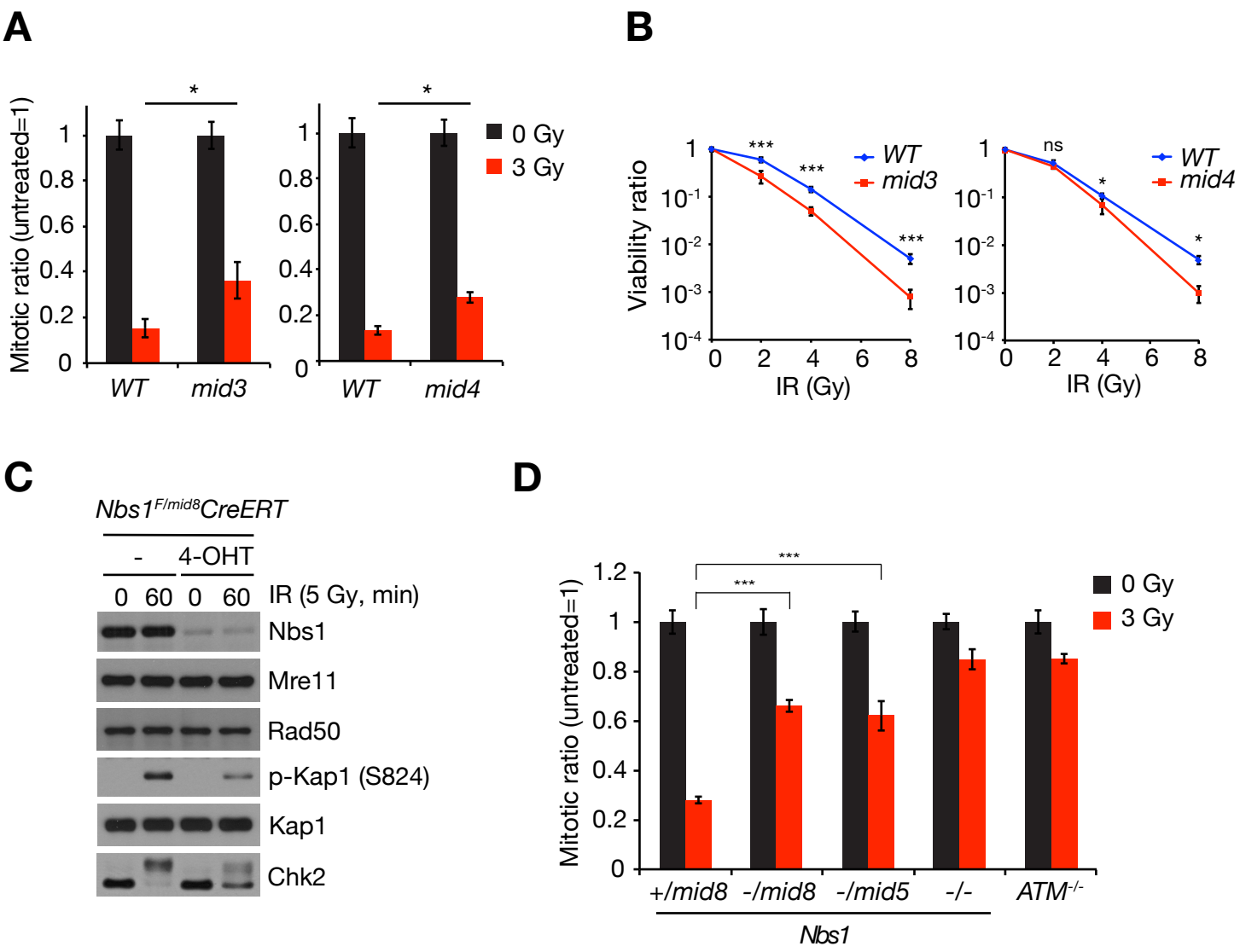

Figure S2. G2/M checkpoint and IR sensitivity of *Nbs1^{mid}* mutants cells, Related to Figure 2. (A) Analysis of G2/M checkpoint in *Nbs1^{mid3}* and *Nbs1^{mid4}* SV40-MEFs. Mitotic cells were detected by measuring mitosis-specific phosphorylation of histone H3 (Ser10). *P-value* was determined by unpaired t-test (*$p<0.05$, mean ± s.d., Two or three independent experiments in triplicate). (B) Colony formation assay to determine the DNA damage sensitivity. *Nbs1^{mid3}* and *Nbs1^{mid4}* SV40-MEFs treated by different dose of IR were grown for 10 days and survived colonies were counted. *P-value* was determined by unpaired t-test (*$p<0.05$, ***$p<0.001$, mean ± s.d., Two or three independent experiments in triplicate). (A and B) *WT* SV40-MEFs generated with littermate embryo of each genotype were used for comparison. (C) ATM signaling in *Nbs1$^{-/mid8}$* SV40-MEFs was assessed by Western blot for the phosphorylation of ATM substrates, KAP1 (S824) and Chk2, after IR treatment. (D) Analysis of G2/M checkpoint in *Nbs1$^{-/mid5}$* and *Nbs1$^{-/mid8}$* SV40-MEFs. Mitotic cells were detected by measuring mitosis-specific phosphorylation of histone H3 (Ser10). *Nbs1$^{+/mid8}$*, *Nbs1$^{-/-}$*, *ATM$^{-/-}$* SV40-MEFs were used for controls. *P-value* was determined by unpaired t-test (***$p<0.001$, mean ± s.d., n=3).

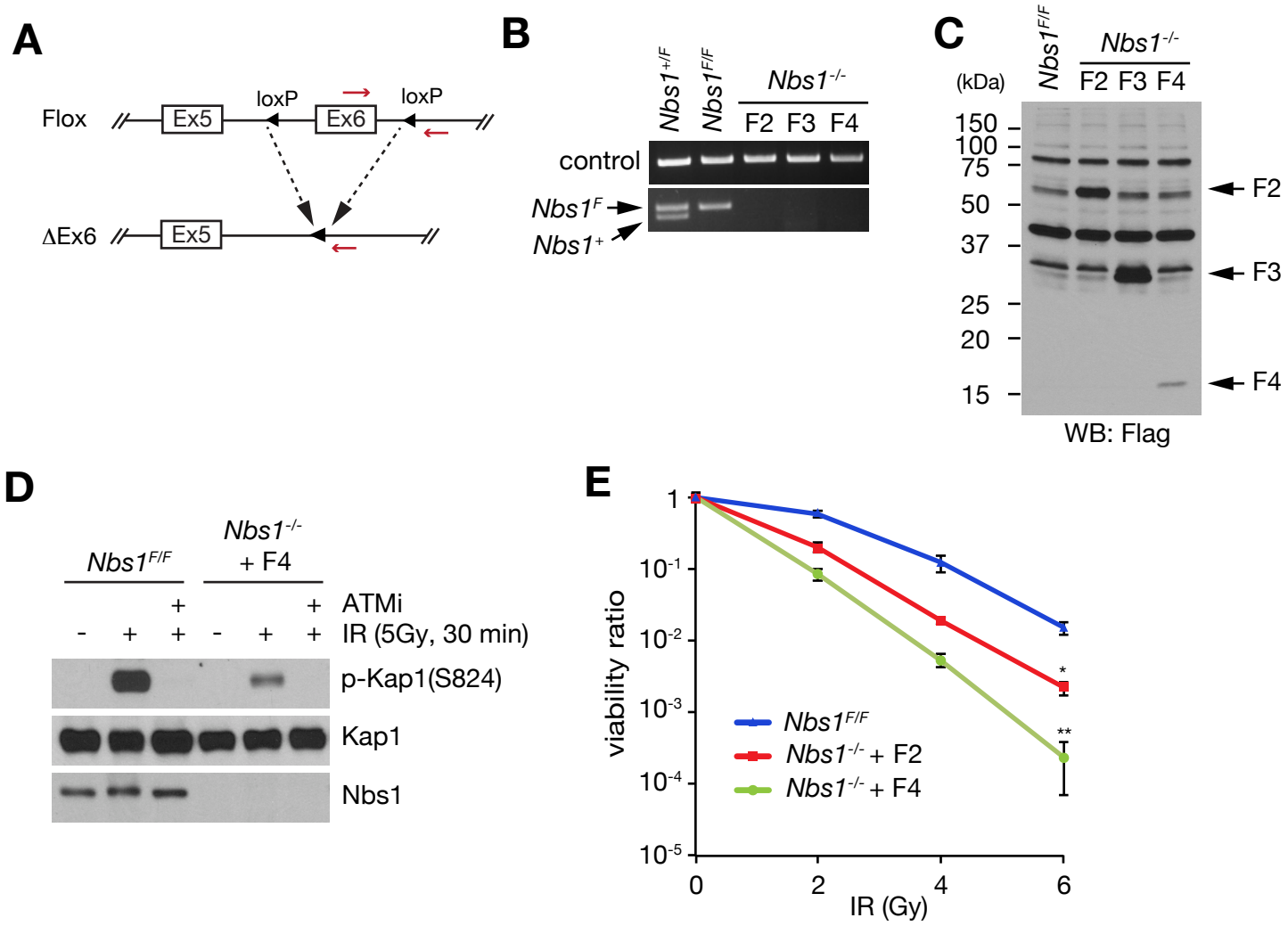

Figure S3. Verification and analysis of rescue cell lines, Related to Figure 3.
(A) *Nbs1*^{F} allele and genotype PCR primers are indicated. Primers are indicated in red arrow and sequences were previously described (Frappart et al., 2005). (B) PCR genotyping of *Nbs1*$^{-/-}$ rescue cells. (C) Expression of rescue fragments was shown by Western blot using anti-Flag antibody. (D) IR-induced p-Kap1(S824) was assessed in the absence or presence of KU-55933 ATM inhibitor (10 μM 1 hr pretreated). Nbs1 level shows the absence of endogenous Nbs1 in *Nbs1*$^{-/-}$ + F4 cells. Colony formation assay to determine the DNA damage sensitivity of *Nbs*$^{-/-}$+ F2 and *Nbs*$^{-/-}$+ F4 SV40-MEFs. Parental *Nbs*$^{F/F}$ SV40-MEFs were used for comparison. Cells treated with different dose of IR were grown for 10 days and survived colonies were counted. *P-value* was determined by unpaired t-test (*$p<0.05$ for *Nbs*$^{F/F}$ vs. *Nbs*$^{-/-}$+ F2; **$p<0.01$ for *Nbs*$^{-/-}$+ F2 vs. *Nbs*$^{-/-}$+ F4, mean ± s.d., Two independent experiments in triplicate).

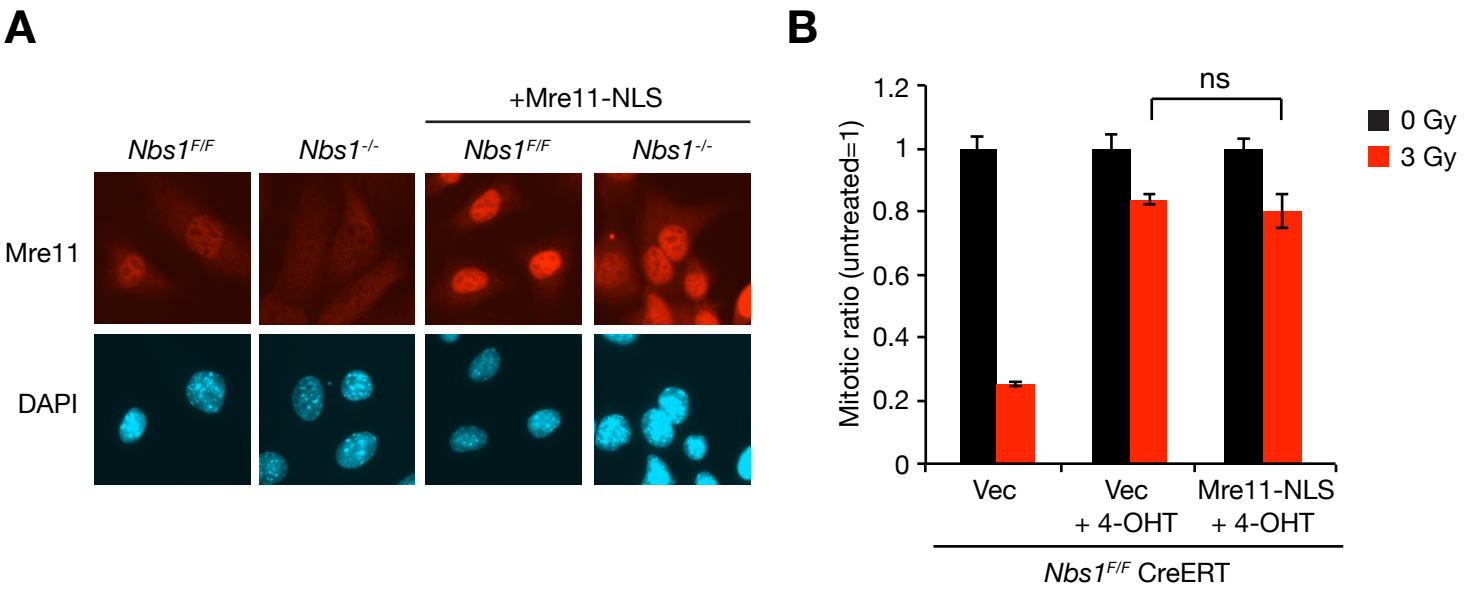

Figure S4. Mre11-NLS expression fails to rescue Nbs1 deficiency, Related to Figure 3. (A) Immunofluorescence cell staining of Mre11-NLS in *Nbs1*$^{-/-}$ SV40-MEFs. Nbs1 deficiency was achieved by cre induction acutely. Nuclei are shown by DAPI (4',6-diamidino-2-phenylindole) staining. (B) IR-induced G2/M cell cycle checkpoint of *Nbs1*$^{-/-}$-Mre11-NLS SV40-MEFs. Mitotic cells were detected by measuring mitosis-specific phosphorylation of histone H3 (Ser10). Three independent clones of *Nbs1*$^{-/-}$-Mre11-NLS SV40-MEFs were analyzed and combined for graph presentation. *P-value* was determined by unpaired t-test (ns: not significant).

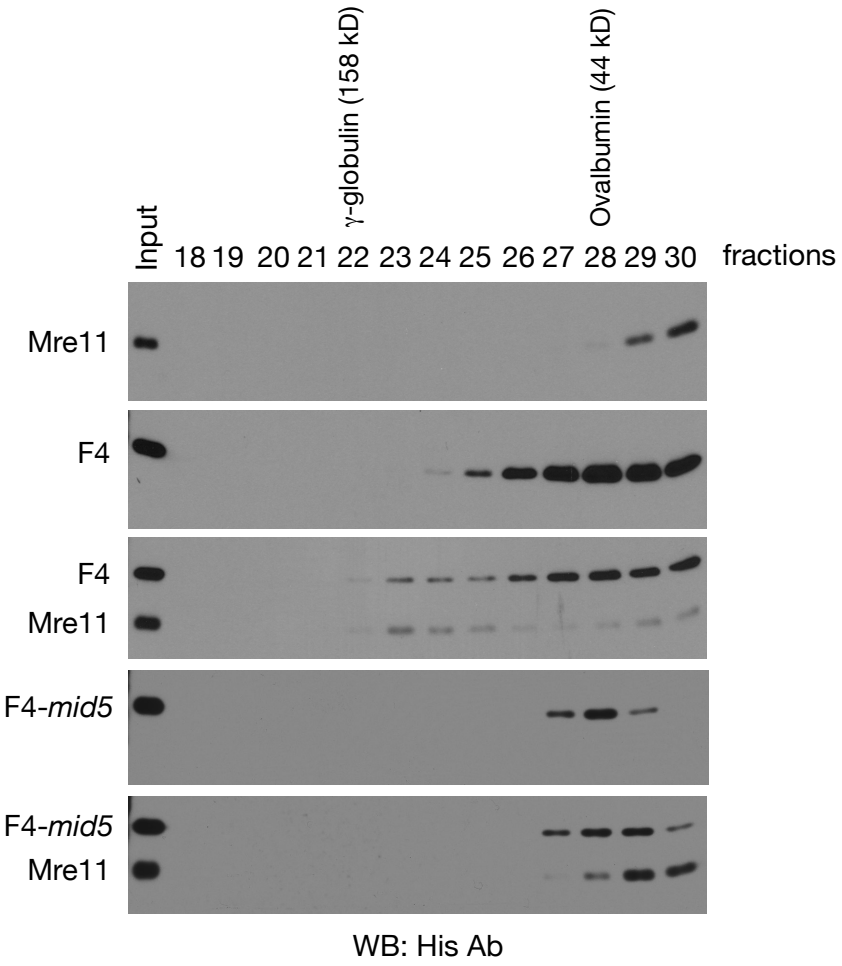

Figure S5. Gel filtration of Mre11 and Nbs1-F4 complex by Superdex 200, Related to Figure 4. Equimolar mixture of human Mre11 (1-411aa) and *WT* or *mid5* Nbs1-F4 protein were used at 0.5 μM. Elution fractions were visualized by Western blot using His antibody. Molecular weight was estimated by gel filtration standard.

Figure S6

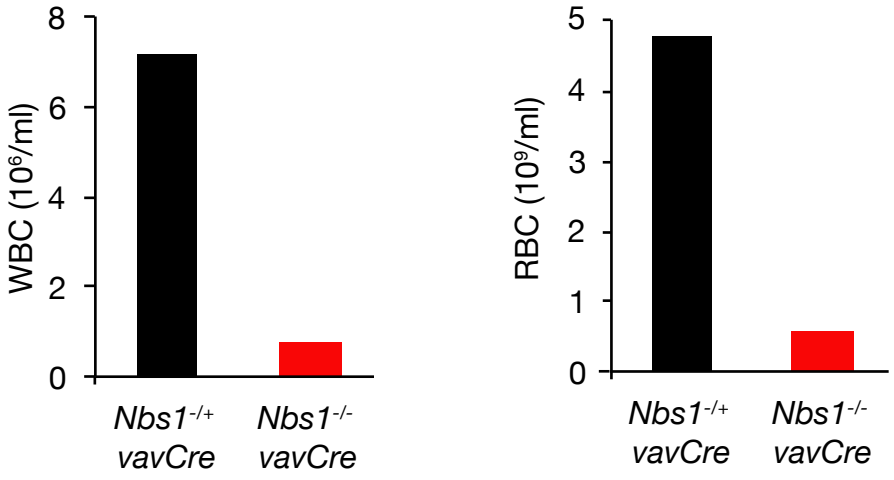

Figure S6. Hemavet quantification of whole blood cell numbers from 12 days-old *Nbs1*$^{-/+}$ *vavCre* and *Nbs1*$^{-/-}$ *vavCre* mice, Related to Figure 6. Peripheral blood from mouse of each genotype was obtained from the tail vein and complete blood cell analysis was performed on Hemavet (Drew Scientific). WBC= white blood cells, RBC=red blood cells.

Table S1. Pathology of *Nbs1*$^{+/+}$ *p53*$^{-/-}$, *Nbs1*$^{mid3/mid3}$ *p53*$^{-/-}$ and *Nbs1*$^{mid4/mid4}$ *p53*$^{-/-}$ mice, Related to Figure 2.

Nbs1$^{+/+}$ *p53*$^{-/-}$

case	Sex	Age (days)	Histological types
1	male	102	lymphoma
2	female	117	ND
3	female	123	lymphoma
4	male	145	lymphoma
5	female	152	lymphoma
6	female	165	lymphoma
7	female	173	lymphoma
8	male	180	lymphoma
9	female	181	ND
10	female	188	lymphoma
11	male	194	lymphoma
12	male	200	lymphoma
13	female	209	lymphoma
14	male	212	lymphoma
15	male	266	lymphoma

Nbs1$^{mid3/mid3}$ *p53*$^{-/-}$

case	Sex	Age (days)	Histological types
1	male	67	leiomyosarcoma
2	male	90	lymphoma
3	female	126	lymphoma, squamous cell carcinoma
4	male	127	lymphoma
5	female	128	lymphoma
6	male	131	lymphoma
7	male	135	lymphoma
8	female	156	lymphoma
9	male	162	lymphoma
10	male	167	lymphoma

Nbs1$^{mid4/mid4}$ *p53*$^{-/-}$

case	Sex	Age (days)	Histological types
1	male	76	lymphoma
2	male	95	lymphoma
3	male	97	lymphoma
4	female	102	lymphoma
5	male	110	hemangiosarcoma
6	male	111	lymphoma
7	male	124	lymphoma
8	male	129	lymphoma
9	male	140	lymphoma
10	male	154	lymphoma
11	female	154	lymphoma
12	male	159	rhabdomyosarcoma
13	male	161	lymphoma
14	male	162	lymphoma
15	female	170	lymphoma
16	male	176	lymphoma
17	male	181	histiocytic sarcoma
18	male	186	lymphoma
19	male	186	lymphoma
20	male	195	ND

ND : not determined.

Supplemental Experimental Procedures

Cell lines

Primary mouse embryonic fibroblasts (MEFs) were derived from E13.5 embryos and maintained in DMEM/10% fetal bovine serum/antibiotics. SV40 transformed MEFs were maintained in DMEM/10% cosmic calf serum.

Inducible MEFs were derived by crossing of *Nbs1*$^{+/mid5\ or\ mid8}$ mice with *Nbs1*^{F} mice. MEFs in which deletion of *Nbs1*^{F} allele is 4-hydroxytamoxifen (4-OHT) inducible were generated by stable expression of MSCV CreERT2 puro (a gift from Tyler Jacks; Addgene plasmid #22776). Deletion was carried out by 1 day exposure with 100 nM 4-OHT treatment followed by removal for additional 3 days to minimize Cre toxicity.

Nbs$^{-/F}$ SV40-MEFs were kindly provided by Titia de Lange (Rockefeller University, USA).

Rescue cells were generated by expression of Flag-SV40 NLS (PKKKRKV) containing Nbs1 fragments followed by deletion of endogenous *Nbs1*^{F} allele. Nbs1 fragments were cloned into pMIG-W-IRES-GFP plasmid (a gift from Luk Parjis; Addgene plasmid #12282). Deletion of endogenous *Nbs1*^{F} allele and expression of exogenous Nbs1 fragments were confirmed by Western blot and PCR genotyping. Mre11-NLS construct was made by insertion of 2 copies SV40 NLS (PKKKRKV) at C terminus of Mre11 cDNA.

Cellular assay

Immunoprecipitaions (IP) were performed with 500 μg of Flag-tagged Nbs1 expressing cells extracts using 1X PBS/0.5% (v/v) TritonX-100/400 mM NaCl/Protease

inhibitor cocktail buffer (Roche). Flag peptide (F3290, Sigma) was added to *WT* sample at 100 μg/ml for a Flag IP control.

Western blots were carried out by standard protocol. Briefly, total cell extracts were prepared in SDS lysis buffer (60 mM Tris-HCl pH 6.8, 2% SDS) and 20-40 μg of extracts were analyzed with specific antibodies. Antibodies used in this study were Mre11 (custom made), Nbs1 (custom made), Rad50 (custom made), p-Kap1 S824 (ab70369, Abcam), total Kap1 (NB500-159, Novus), Chk2 (05-649, Millipore), p-ATM S1981 (#4526L, Cell signaling), total ATM (#2873S, Cell signaling), and Flag (F3165, Sigma).

G2M cell cycle checkpoint assay was performed by flow cytometry measuring Ser10 phosphorylation of histone H3 with anti-phospho-Ser10-Histone H3 antibody (06-570, Millipore) 1 hr after 3 Gy of IR exposure.

For colony formation assay, cells were plated with different IR treatments and cultured for 10 days. Colonies were visualized by crystal violet stain and counted.

For micronuclei staining, cells were fixed with 4% (v/v) formaldehyde in PBS for 15 min at RT and permeabilized in PBS containing 0.5% (v/v) TritonX-100. Cells were mounted with ProLong® Gold Antifade DAPI-Mountant (Life technologies).

For metaphase spread, cells were treated with 100 ng/ml of KaryoMAX colcemid (Life technologies) for 1 hr and harvested. Cells were swelled in 0.075 M KCl for 15 min at 37°C and fixed in ice-cold 3:1(v/v) methanol: acetic acid. Dropped samples on slides were stained with 5% Giemsa (Sigma) and mounted with Permount medium (Fisher Scientific). More than 40 spreads were analyzed per each sample.

Fetal liver cell (FLC) transplantation

For donor FLCs, fetal liver cells were isolated from E13.5 *Nbs1$^{F/F}$vavCre* embryos and red blood cells were lyzed in ACK lysis buffer (150 mM NH_4Cl, 10 mM $KHCO_3$, 0.1 mM EDTA). FLCs were maintained in FLC media (DMEM-IMDM1:1/10% FBS/4 mM L-glutamine/50 mM β-mercaptoethanol, 10 ng/ml IL-3, 10 ng/ml IL-6, 20 ng/ml SCF). For transplantation, donor *Nbs1$^{F/F}$vavCre* FLCs were infected by spin infection (1800 rpm for 45 min with 8 μg/ml of polybrene) with retrovirus expressing Nbs1 fragment-IRES-GFP. As the viability of *Nbs1$^{F/F}$vavCre* FLCs dropped during the culture after isolation, cells were infected and cultured only for 3 days before transplantation. Due to the mouse strain of donor *Nbs1$^{F/F}$vavCre* FLCs, we used F1 hybrid of C57BL/6 x 129 as a recipient. Briefly, 6-week old F1 hybrid mice were irradiated at lethal dose (5 Gy x 2 times) and 3×10^5 FLCs were transplanted via tail vein injection. After 10 weeks post transplantation, thymocytes and splenocytes were isolated and analyzed to assess GFP^+ cells that were derived from donor FLCs expressing Nbs1 fragment-IRES-GFP. Rescued cells by Nbs1 fragment-IRES-GFP were confirmed by flow cytometry and PCR genotyping using primers for *vavCre* or exogenous Nbs1 rescue fragments that are specific for donor cells. Primers for PCR genotyping are *vavCre* allele and Nbs1 rescue fragments are 5'-CAAGTGACAGCAATGCTGTTTCAC-3', 5'-CAGGTATCTCTGACCAGAGTCATC-3' for Cre and 5'-CAGTGAGGAGCTGCCACGGAAACT-3', 5'-TCTAACTCGGTATTCTTTCGAGCATGGT-3' for Nbs1 rescue fragments.

Protein purification and analysis

Bacterial expression vector for N-terminal his-tagged human Mre11 (2-411aa) was gifted from Dr. John Tainer (Lawrence Berkeley National Laboratory, USA). With C-

terminal his-tag, human Nbs1 (F4, 622-729aa) was constructed in pMAL vector (New England BioLabs) for N-terminal MBP-tag for its solubility.

For purification, Mre11 protein was purified by serial FPLC purification using HisTRAP (GE Healthcare) and HiTRAP Q FF (GE Healthcare) column followed by Superdex S200 (GE Heathcare) gel filtration. FPLC running buffers are; 20 mM Tris-HCl pH8, 0.5 M NaCl, 0.5 mM DTT, 5 mM imidazole for HisTRAP; 20 mM Tris-HCl pH 8, 0.1 mM EDTA, 2 mM DTT for HiTRAP Q FF ; 20 mM Tris-HCl pH 8, 0.1 mM EDTA, 0.2 M NaCl, and 2 mM DTT for Superdex S200. Nbs1 proteins were purified by batch affinity purification methods using amylose resin (New England BioLabs) followed by Nickel-affinity purification (Qiagen) by manufacturer's standard protocol. Then, the samples were subject to FPLC Superdex S200 gel filtration to remove imidazole from the elution buffer. Mre11 and Nbs1 proteins were eluted at the single peak as a monomer at the given gel filtration condition.

For electrophoretic mobility shift assay (EMSA), the indicated amounts of purified Mre11 and Nbs1 proteins were incubated with ^{32}P-end labeled dsDNA or hairpin DNA probe in the binding condition of 25 mM Tris-HCl pH8, 100 mM NaCl, 1 mM DTT for 20 min at RT. The sequences of ds DNA is 5'-GTCTTCAGGACAGCAGTGAGGAGAACCCACGGAAACTGCTGCTGACTGA-3', and hairpin is 50 nt (DAR134) previously used (Paull and Gellert, 1998). The reactions were loaded in to 5% native-PAGE and run for 1hr at 200 V in 0.5x TBE buffer. After drying gel, the probes in the gel were visualized by phosphorimager (Fujifilm). For supershift, 1 μg of MBP (sc-32747, Santa Cruz) or control antibodies (sc-2025, Santa Cruz) were preincubated 10 min at RT before adding DNA probe.

Nuclease assay

Nuclease assay were performed as described in previous literatures (Anand et al., 2016; Cannavo and Cejka, 2014). Briefly, 3'-end radiolabelled 1 nM of biotinylated 70 bp-long DNA oligonucleotide substrates were incubated with streptavidin (15 nM, Sigma) to block the ends of substrates. Purified recombinant proteins were then added to the reaction for 30 min at 30°C in nuclease reaction buffer containing 25 mM Tris-acetate pH 7.5, 25 mM Manganese acetate, 1 mM Magnesium acetate, 5 mM Dithiothreitol, 1 mM ATP, 1 mM Bovine serum albumin (New England Biolabs), 0.25 mg/ml Phosphoenolpyruvate, and 1 mM Pyruvate kinase (Sigma). Reaction products were analyzed on 15 % polyacrylamide denaturing urea gels (19:1 acrylamide-bisacrylamide, Bio Rad) and scanned by Typhoon phosphor imager (GE Healthcare).

Immunofluorescence staining

Cells were fixed with 4% (v/v) formaldehyde in PBS for 15 min at RT and permeabilized in PBS containing 0.5% (v/v) TritonX-100. All staining were done with PBS buffer containing 1% BSA, 0.1% (v/v) Tween 20. Primary antibodies were used at 1:10000 (Mre11; custom made) or 1:2000 (Rad50; IHC-00076, Bethyl) and secondary antibodies (Alex Fluor-594; Life technologies) were used at 1:1000 dilutions. Cells were mounted with ProLong® Gold Antifade DAPI-Mountant (Life technologies).

Histopathology

Tissue samples from the sacrificed mice were fixed with 4% (v/v) formaldehyde overnight at 4°C and stored at 4°C in 70% ethanol. Paraffin embedded samples were prepared by eight-micrometer section and were subjected to pathological analysis

after Hematoxylin and eosin (H&E) staining. All sample preparation and pathological analysis were performed by Histoserv, Inc. (Maryland, USA).

Supplemental References

Anand, R., Ranjha, L., Cannavo, E., and Cejka, P. (2016). Phosphorylated CtIP Functions as a Co-factor of the MRE11-RAD50-NBS1 Endonuclease in DNA End Resection. Mol Cell. doi: 10.1016/j.molcel.2016.10.017.

Cannavo, E., and Cejka, P. (2014). Sae2 promotes dsDNA endonuclease activity within Mre11-Rad50-Xrs2 to resect DNA breaks. Nature *514*, 122-125.

Frappart, P.O., Tong, W.M., Demuth, I., Radovanovic, I., Herceg, Z., Aguzzi, A., Digweed, M., and Wang, Z.Q. (2005). An essential function for NBS1 in the prevention of ataxia and cerebellar defects. Nature medicine *11*, 538-544.

Paull, T.T., and Gellert, M. (1998). The 3' to 5' exonuclease activity of Mre 11 facilitates repair of DNA double-strand breaks. Mol Cell *1*, 969-979.